Copyright Warning & Restrictions

The copyright law of the United States (Title 17, United States Code) governs the making of photocopies or other reproductions of copyrighted material.

Under certain conditions specified in the law, libraries and archives are authorized to furnish a photocopy or other reproduction. One of these specified conditions is that the photocopy or reproduction is not to be "used for any purpose other than private study, scholarship, or research." If a, user makes a request for, or later uses, a photocopy or reproduction for purposes in excess of "fair use" that user may be liable for copyright infringement,

This institution reserves the right to refuse to accept a copying order if, in its judgment, fulfillment of the order would involve violation of copyright law.

Please Note: The author retains the copyright while the New Jersey Institute of Technology reserves the right to distribute this thesis or dissertation

Printing note: If you do not wish to print this page, then select "Pages from: first page # to: last page #" on the print dialog screen

NJIT New Jersey's Science & Technology University

The Van Houten library has removed some of the personal information and all signatures from the approval page and biographical sketches of theses and dissertations in order to protect the identity of NJIT graduates and faculty.

ABSTRACT

ELECTRICAL, ELECTRONIC and OPTICAL PROPERTIES OF $MoSe_2$ and WSe_2

By

Sushant Shashikant Rassay

Transition-metal dichalcogenides (TMDC) crystals have emerged as a new class of semiconductors that display distinctive properties at monolayer thickness. Their electrical, electronic and optical properties are of particular interest and importance for applications in optoelectronics as light emitters, detectors, and photovoltaic devices. Monolayer $MoSe_2$ and WSe_2 have an intrinsic band-gap in the visible region of the solar spectrum (400nm – 700nm) which makes them distinct from other 2-D materials like graphene.

In this study, the electrical, electronic and optical properties of monolayer and bulk $MoSe_2$ and WSe_2 are studied. The electronic band structures are presented for monolayer and bulk $MoSe_2$ and WSe_2. The optical properties of $MoSe_2$ and WSe_2 comprises of the determination and analysis of the spectral properties of these materials, at monolayer and bulk, in the range of 1.50 - 3.0 eV by MATLAB simulations. The optical band gaps of TMDC monolayers have been simulated from their spectral dependence of the absorption coefficient. The optical properties of these materials on silicon, gold and fused silica substrates are simulated.

ELECTRICAL, ELECTRONIC and OPTICAL PROPERTIES OF $MoSe_2$ and WSe_2

By
Sushant Shashikant Rassay

A Thesis
Submitted to the Faculty of
New Jersey Institute of Technology
in Partial Fulfillment of the Requirements for the Degree of
Master of Science in Materials Science and Engineering

Interdisciplinary Program in Materials Science and Engineering

January 2017

APPROVAL PAGE

ELECTRICAL, ELECTRONIC and OPTICAL PROPERTIES OF $MoSe_2$ and WSe_2

Sushant Shashikant Rassay

Dr. N. M. Ravindra, Thesis Advisor — Date
Professor, Department of Physics, NJIT

Dr. Yuanwei Zhang, Committee Member — Date
Assistant Professor, Department of Chemistry and Environmental Science, NJIT

Dr. Michael Jaffe, Committee Member — Date
Research Professor, Department of Biomedical Engineering, NJIT

BIOGRAPHICAL SKETCH

Author: Sushant Shashikant Rassay

Degree: Master of Science

Date: January 2017

Undergraduate and Graduate Education:

- Master of Science in Materials Science and Engineering,
  New Jersey Institute of Technology, Newark, NJ, 2017

- Bachelor of Technology in Electronics Engineering,
  Vishwakarma Institute of Technology, Pune, Maharashtra, India, 2014

Major: Materials Science and Engineering

I would like to dedicate this work to
my parents, Mr Shashikant Prabhakar Rassay and Mrs. Shrutika Prabhakar Rassay,
my family, Mr. Shantanu Shashikant Rassay,
and my mentor, Dr. Chandrashekhar Mahajan
for their continuous support and motivation in my life !

ACKNOWLEDGMENT

I would like to thank Dr. N. M. Ravindra, with immense gratitude, as an advisor, for his continuous support, invaluable insights and inspiration during the entire course of research. His guidance at all times has been of enormous value. Without his excellent advice and guidance on this topic, this work could not have been accomplished. I would like to sincerely thank my committee members Dr. Michael Jaffe and Dr. Yuanwei Zhang.

I acknowledge with thanks the valuable input from Ms. Clarisa Gonzalez-Lenahan, Associate Director of Graduate Studies and Mrs. Lillian Quiles, the Administrative Assistant for formatting and improving the presentation of my thesis.

I would like to thank my research group member Weitao Tang for his support in various aspects during my stay in NJIT.

I am highly indebted to my father, Mr. Shashikant P. Rassay and my mother Mrs. Shrutika S. Rassay for being the pillar of my support and blessing throughout my life. I would like to express my gratitude to my sibling, Shantanu S. Rassay. I would like to thank my mentor Dr Chandrashekar Mahajan who helped me in every academic aspect of my life and gave me the confidence and knowledge to reach new levels.

TABLE OF CONTENTS

TABLE OF CONTENTS
(Continued)

Chapter **Page**

TABLE OF CONTENTS
(Continued)

LIST OF FIGURES

LIST OF FIGURES
(Continued)

LIST OF FIGURES
(Continued)

Figure **Page**

LIST OF TABLES

CHAPTER 1

INTRODUCTION

In this thesis, the electrical, electronic and optical properties of $MoSe_2$ and WSe_2 are investigated. The details of this study are presented in six chapters.

The second Chapter deals with the physical structures of $MoSe_2$ and WSe_2. The fundamental properties such as lattice parameters and crystal structure of $MoSe_2$ and WSe_2 are explained in detail.

The third Chapter of this thesis deals with the electronic properties of $MoSe_2$ and WSe_2. The dependence of temperature on the energy gap of monolayer $MoSe_2$ and WSe_2 is also presented in this chapter. A literature survey of the band structures of monolayer and bulk $MoSe_2$ and WSe_2 are discussed in this Chapter; the literature survey focuses on the band gap transitions in $MoSe_2$ and WSe_2.

The fourth Chapter focuses on the electrical properties of $MoSe_2$ and WSe_2. Properties such as resistivity, sheet resistance, Hall effect, Ohmic nature and doping concentrations are discussed in this chapter.

The fifth Chapter deals with the optical properties of $MoSe_2$ and WSe_2. In this Chapter, optical constants (n – refractive index and k – extinction coefficient), optical properties (Reflectance, Transmittance and Absorptance) of monolayer and bulk $MoSe_2$ and WSe_2 under conditions of normal incidence are presented. The optical properties of these materials on gold, silicon and fused silica are presented in this Chapter. All the optical properties and optical constants were computed using MATLAB simulations.

The sixth Chapter focuses on the potential applications of $MoSe_2$ and WSe_2. The existing applications, reported in the literature, are discussed in this Chapter.

The seventh Chapter is the conclusion and recommendations followed by the references. The Appendix consists of the MATLAB code used to run the simulations.

CHAPTER 2

OVERVIEW

The discovery of graphene started a revolution in the field of materials science and engineering and proved to be a building block for nano-structures and carbon nanotubes. Its stable 2-D structure and ease of production caused a stir in the scientific society. However, Graphene's gapless electronic structure limited its applications in the field of nano-electronics and optoelectronics; this led scientists and researchers to probe into the world of semiconducting 2-D materials.

Transition Metal Dichalcogenides (TMDCs) are a group of 2-D materials, which have garnered unprecedented attention due to their layered structure and indirect and direct band gap transitions. This property distinguishes them from the more prominent graphene. Due to the presence of an indirect band gap, these materials find their applications in the field of semiconductor devices as switches. TMDCs show distinct properties at the monolayer level than compared to the bulk level.

In recent years, extensive research has been performed on MoS_2; this is due to the abundance of molybdenite and the stable nature of bulk and monolayer MoS_2. MoS_2 possesses physical properties that are most relevant in device applications such as field-effect transistors (FETs), memory devices, photodetectors, solar cells, electrocatalysts for hydrogen evolution reaction (HER) and lithium ion batteries [1].

2.1 Physical Properties of $MoSe_2$ and WSe_2

The transition-metal dichalcogenides, MX_2, where 'M' is a transition metal and 'X', a chalcogen, have been investigated for fullerene-like behavior due to their tendency to form layered structures. A single layer consists of a strongly bound X-M-X sandwich that is weakly stacked with other layers. The crystal structures vary in the number of layers per unit cell and the alignment of the layers with respect to one another [2].

$MoSe_2$ and WSe_2 are layered materials with strong in-plane bonding and weak out-of-plane interactions enabling exfoliation into two-dimensional layers of single unit cell thickness. Although TMDCs have been studied for decades, recent advances in nanoscale materials characterization and device fabrication have opened up new opportunities for two-dimensional layers of thin TMDCs in nanoelectronics and optoelectronics. $MoSe_2$ and WSe_2 have sizable bandgaps that change from indirect to direct in single layers, allowing applications such as transistors, photodetectors and electroluminescent devices. Adjacent layers are weakly held together to form the bulk crystal in a variety of polytypes, which vary in stacking orders and metal atom coordination. The overall symmetry of TMDCs is hexagonal or rhombohedral, and the metal atoms have octahedral or trigonal prismatic coordination [3].

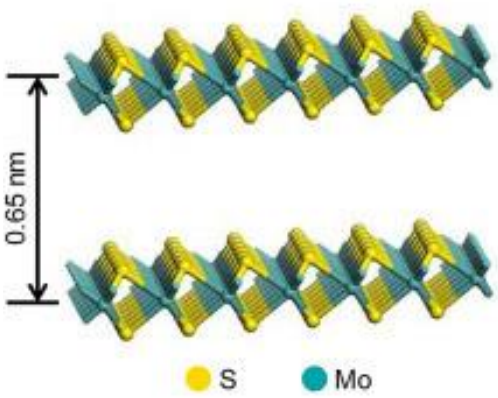

Figure 2.1 Structure of monolayer MoS_2.

Source: Li, Xiao, and Hongwei Zhu. "Two-dimensional MoS_2: Properties, preparation, and applications." *Journal of Materiomics* 1.1 (2015): 33-44.

Figure 2.1 depicts the structure of monolayer MoS_2 that has an interlayer spacing of 0.65 nm. $MoSe_2$ and WSe_2 also have a physical structure similar to that of MoS_2, the only difference being the interlayer spacing. Difference in the atomic size of 'Mo' and 'W' results in a change in the interlayer spacing.

$MoSe_2$ and WSe_2 portray different properties at the monolayer and bulk levels. At the bulk level, these materials have an indirect bandgap, whereas, at a monolayer level the band gap increases for both, $MoSe_2$ and WSe_2 [3]. Because of these layer dependence properties, the monolayer and bulk crystal structures of $MoSe_2$ and WSe_2 are examined. Monolayer WSe_2 has a thickness of ~0.7 nm and bulk WSe_2 has a thickness of ~20 nm. These are experimental values and have been obtained by various deposition techniques such as Chemical Vapor Deposition (CVD) and mechanical exfoliation of bulk WSe_2 crystals [4].

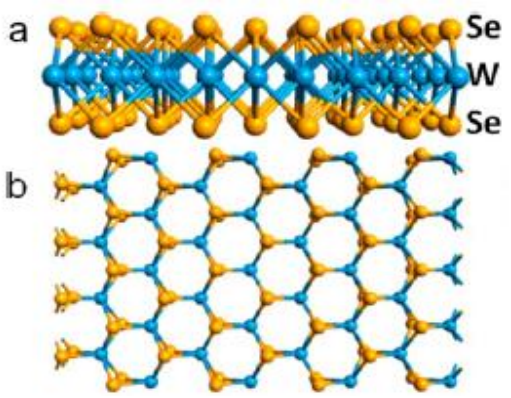

Figure 2.2 Schematic of the crystal structure of monolayer WSe_2, (a) side view and (b) top view.

Source: Liu, W., Kang, J., Sarkar, D., Khatami, Y., Jena, D., & Banerjee, K. (2013). Role of metal contacts in designing high-performance monolayer n-type WSe_2 field effect transistors. Nano letters, 13(5), 1983-1990.

Figure 2.2 shows the crystal structure of monolayer WSe_2, the inter layer distance between Se-W-Se bonds is ~0.7 nm and is also the thickness of the monolayer. As seen in the figure, the Se-W-Se bonds form a hexagonal symmetry and is hence of 3H form. Bulk structure of WSe_2 is formed by stacking multiple monolayers of WSe_2; the thickness of these structures is generally ~20 nm. Usually, bulk WSe_2 crystals consist of weakly bonded Se-W-Se units (three atomic planes) [4].

The crystal structure of $MoSe_2$ is similar to that of WSe_2 as the only difference being the transition metal atom, which leads to a minor change in the monolayer thickness. Just like monolayer WSe_2, in monolayer $MoSe_2$ 'Mo' and 'Se' atoms form a 2D hexagonal lattice with trigonal prismatic coordination as shown in Figure 2.3 [5].

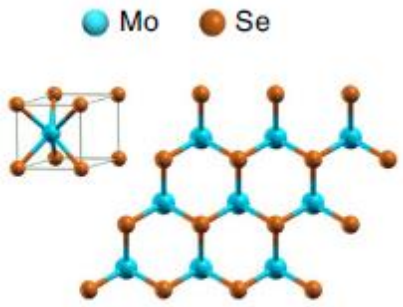

Figure 2.3 Coordination structure and crystal structure of monolayer $MoSe_2$.

Source: Ross, J. S., Wu, S., Yu, H., Ghimire, N. J., Jones, A. M., Aivazian, G., & Xu, X. (2013). Electrical control of neutral and charged excitons in a monolayer semiconductor. *Nature communications*, *4*, 1474.

In $MoSe_2$, the 'Mo' atoms occupy one type of sub-lattices of the hexagonal sheet and atoms of 'Se' occupy the others. However, due to the chemical ratio of Mo: Se = 1:2, the sub-lattice layer of element 'Mo' is sandwiched between two nearby 'Se' sub-lattice layers. In a perfect $MoSe_2$ monolayer, 'Mo' and 'Se' atoms alternately connect each other, forming only Mo-Se bonds [6].

A few of the physical properties such as melting point, lattice parameters, electron concentration etc. are summarized in Table 2.1.

Table 2.1 Physical Properties of 2H-$MoSe_2$ and WSe_2

Material	Lattice Parameter	Melting Point	Energy Gap	Effective hole mass	Electron concentration
2-H $MoSe_2$	a = 3.288 Å c = 12.92 Å	1473 K	1.60 eV (direct) 0.95 eV (indirect)	_____	$0.35\text{-}1.6\cdot10^{17}$ cm^{-3} single crystal
2-H WSe_2	a = 3.282 Å c = 12.937 Å	1773 K	1.73 eV (direct) 1.33 eV (indirect)	0.01 m_0	$1.25\cdot10^{16}$ cm^{-3} single crystal
References	7	8	9	10	

CHAPTER 3

ELECTRONIC PROPERTIES OF $MoSe_2$ and WSe_2

3.1 General Considerations

Understanding the electronic properties of a material opens a gateway to other properties that are exhibited by the material. It is important to know the band gap, band gap transitions, lattice structure and lattice parameters of the material. Based on the results obtained, we can further posit on its potential applications in various fields of science. In order to know if a material is a conductor, semiconductor or insulator, we must know the position of the band gaps and the valleys present in it. The examination of quantum mechanical wave functions of a particular electron in a vast lattice of atoms or molecules forms the basis for determining the band structure.

In a band structure, the wave function is denoted with a quantum number ‘n’ and the wave vector ‘k’. Each value of ‘k’ has a discrete spectrum of states, labeled by band index ‘n’, the energy band numbering. The number of bands, in a band structure diagram, is equal to the number of atomic orbitals in the unit cell [11]. The overlap integral determines the width of the band. This is the difference in the energy between the lowest and highest points in a band. The greater the overlap between neighboring unit cells, the greater is the bandwidth and vice versa [11]. The wave vector ‘k’ can take any value within the Brillouin zone. All the points in a Brillouin zone can be classified using the symmetry of the reciprocal lattice. Symmetric points or Lifschitz points [12], also called

special/specific high symmetry points, are those points which remain fixed or transform into an equivalent one under a symmetry operation of the Brillouin zone. These points play a specific role in solid state physics: (a) if two ‘k’ vectors can be transformed into each other due to some set of symmetry elements, electronic energies at those k-vectors must be identical; (b) “wave functions can be expressed in a form such that they have definite transformation properties under symmetry operations of the crystal” [13]. Similarly, we can define symmetric lines and planes in the Brillouin zone. Customarily, Greek letters denote high symmetry points and lines inside the Brillouin zone while Roman letters denote those on the surface. The center of a Brillouin zone is always denoted by Greek letter ‘Γ’. The behavior of electrons in a solid can be studied microscopically from its electronic band structure [13].

There are various approaches to determine the band structure of material. Some of them maybe, Density functional theory, Green – Kubo relations, Linear Density Approximations (LDA) and so on. The Density Functional Theory is a computational quantum mechanical modelling method used in physics, chemistry and materials science to investigate the electronic structure (principally the ground state) of many-body systems, in particular atoms, molecules, and the condensed phases. Using this theory, the properties of a many-electron system can be determined by using functionals such as spatially dependent electron density. It is among the most popular and versatile methods available in condensed-matter physics, computational physics, and computational chemistry.

In this section, the electronic properties of $MoSe_2$ and WSe_2 have been discussed. The electronic properties include electronic band structure, optical band gap and the influence of temperature on the band gap.

3.2 Electronic Band Structure of $MoSe_2$

The presence of a direct band gap in monolayer $MoSe_2$ and WSe_2 makes it a good candidate for applications in the field of electronics. Monolayer $MoSe_2$ has a direct band gap at monolayer thickness, but the band gap changes to an indirect band gap with the increase in thickness of the monolayer. Hence, bulk $MoSe_2$ and WSe_2 have an indirect band gap. This apparent transition in the band gap causes a variation in the optical properties of monolayer and bulk TMDCs. The band structures presented in this study are a literature survey of existing research work on the electronic properties of TMDCs. Most of the simulations and modelling are done using the Linear Density Approximation (LDA) and Density Functional Theory (DFT) techniques.

The electronic structure of a material involves determining the lattice parameters, Brillouin zone identification and calculation of density of states. Lattice parameters of a monolayer and bulk orientations do not differ by much as monolayer TMDC is obtained from mechanical exfoliation of the bulk counterpart [14].

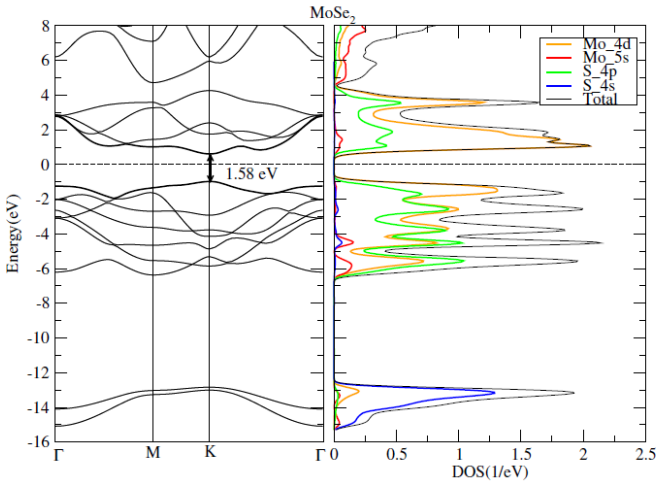

Figure 3.1 Electronic band structure and corresponding total and partial density of states of 1H-$MoSe_2$ (Monolayer).

Source: Kumar, A., & Ahluwalia, P. K. (2012). Electronic structure of transition metal dichalcogenides monolayers 1H-MX2 (M= Mo, W; X= S, Se, Te) from ab-initio theory: new direct band gap semiconductors. The European Physical Journal B, 85(6), 1-7.

The electronic band structure, presented in Figure 3.1, shows the results of the simulation by Kumar et al. [14], The Fermi level is set to 0 eV and all the partial density of states are multiplied by 1.5. As observed from the figure, the direct band gap is found to be 1.58 eV and is close to the theoretical value of 1.60 eV stated in Table 2.1. The direct band gap is observed at a 'K' high symmetry point.

The electronic bands and density of states around −12 eV to −15 eV are mainly derived from the chalcogen 's' orbitals separated by a large gap from the group of electronic bands and density of states below the band gap. The region up to 6–8 eV below the band gap in the valence bands and the region above the band gap are mainly contributed by 'p' orbitals of chalcogens and 'd' orbitals of transition metals [14]. The bands on each side of the band gap originate primarily from the 'd' states of transition metals. Strong

hybridization between ‘d’ states of metal atoms and s states of chalcogen atoms were found below the Fermi energy for all the compounds considered in the study [14].

As reported by Kumar et al. [14] and a few other papers, a band gap transition is observed for bulk and monolayer $MoSe_2$. At its bulk phase, $MoSe_2$ is an indirect band gap semiconductor. The author also reports a blue shift in its indirect band gap while transitioning from the bulk phase to the monolayer limit. The band gap of bulk $MoSe_2$ is in the infrared region. For the monolayer, it shifts towards the near infrared and visible regions. Thus, a change is observed in the electronic properties of $MoSe_2$ from being an indirect semiconductor in the bulk phase to direct semiconductor in the monolayer limit [14].

The electronic band structure of bulk $MoSe_2$ is shown in Figure 3.2. The arrow points to the lowest value of the indirect or direct band gap.

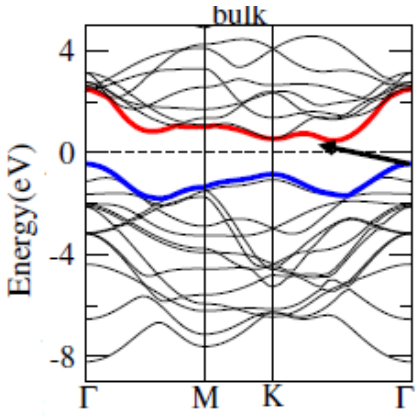

Figure 3.2 Electronic band structure of 2H-$MoSe_2$.

Source: Kumar, A., & Ahluwalia, P. K. (2012). Electronic structure of transition metal dichalcogenides monolayers 1H-MX2 (M= Mo, W; X= S, Se, Te) from ab-initio theory: new direct band gap semiconductors. The European Physical Journal B, 85(6), 1-7.

Figure 3.3 shows the variation of indirect band gap energies (solid lines with triangles) and direct band gap energies at the 'K' point (solid line with circles). The horizontal dotted line and solid line indicates the direct gap at the 'K' point and indirect gap respectively for bulk materials.

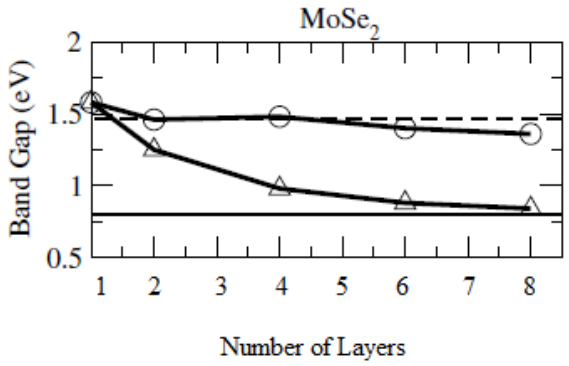

Figure 3.3 Variation of indirect band gap energies (solid lines with triangles) and direct band gap energies at the 'K' point (solid lines with circles) for $MoSe_2$.

Source: Kumar, A., & Ahluwalia, P. K. (2012). Electronic structure of transition metal dichalcogenides monolayers 1H-MX2 (M= Mo, W; X= S, Se, Te) from ab-initio theory: new direct band gap semiconductors. The European Physical Journal B, 85(6), 1-7.

3.3 Electronic Band Structure of WSe_2

The evolution in the band structure of WSe_2 involves direct and indirect band gap transitions. Monolayer WSe_2 has a direct band gap while bulk WSe_2 as an indirect band gap due to transition with increasing layer thickness. As mentioned in Table 2.1, its direct band gap is 1.73 eV and indirect band gap is 1.33 eV. However, these values differ from author to author and depend on the approximation techniques and theoretical approach used.

Figure 3.4 shows the electronic band structure and density of states of monolayer WSe_2. Linear density approximation was used to compute the electronic band structure.

Direct band gap was observed at 1.61 eV, which is close to the theoretical value of 1.73 eV mentioned in Table 2.1.

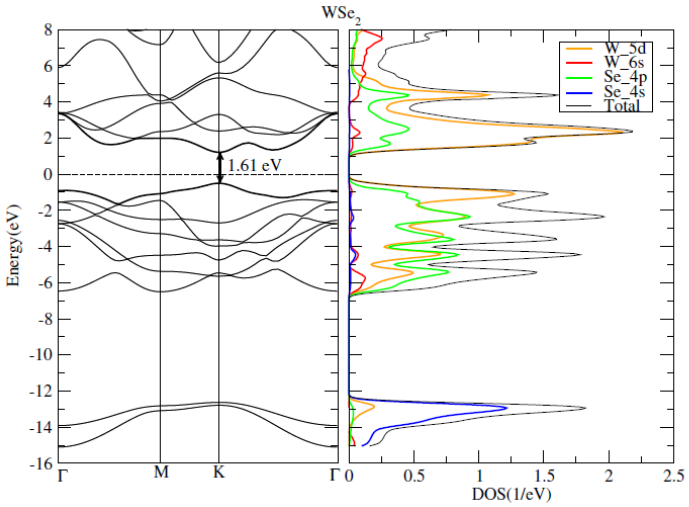

Figure 3.4 Electronic band structure and corresponding total and partial density of states of 1H-WSe_2.

Source: Kumar, A., & Ahluwalia, P. K. (2012). Electronic structure of transition metal dichalcogenides monolayers 1H-MX2 (M= Mo, W; X= S, Se, Te) from ab-initio theory: new direct band gap semiconductors. The European Physical Journal B, 85(6), 1-7.

From Figure 3.4, we observe that the valence band maximum and the conduction band minimum are located at the 'K' point. The indirect-direct band gap transitions have been attributed to the missing interlayer interactions in monolayer MX_2 [15]. It has been reported that monolayer WSe_2 has the largest splitting size amongst all the MX_2 semiconductors. Due to the strong spin−orbit coupling and inversion symmetry breaking, a spin split structure arises, hence contributing to a key property of MX_2 semiconductors [16]. The spin orbit coupling in tungsten is large compared to that molybdenum, and hence, monolayer WSe_2 finds its applications in the field of spintronics [17].

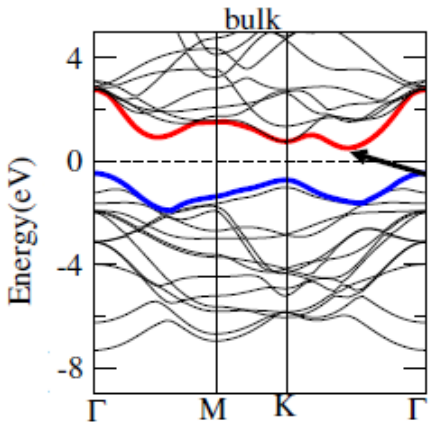

Figure 3.5 Electronic band structure of bulk WSe_2.

Source: Kumar, A., & Ahluwalia, P. K. (2012). Electronic structure of transition metal dichalcogenides monolayers 1H-MX2 (M= Mo, W; X= S, Se, Te) from ab-initio theory: new direct band gap semiconductors. The European Physical Journal B, 85(6), 1-7.

Figure 3.5 depicts the electronic band structure of bulk WSe_2; the arrow points to the lowest value of indirect or direct band gap, while the bottom of the CB and top of VB are highlighted with red and blue, respectively [14].

Zhang et al. [17] reported observation of direct-indirect transition for monolayer, bilayer and trilayer WSe_2. The use of angle-resolved photoemission spectroscopy (ARPES) enabled them to produce and focus on the band structure spectra of the valence band maximum. The top of the VB at the 'Γ' point was slightly larger than the 'K' point; this suggested a direct to indirect band gap transition in WSe_2 between bilayer and trilayer levels [17]. The ARPES spectra also showed that the valence band at the 'K' point split into two branches, which had an energy difference of ~ 475 meV, which was found to be higher than the values found for other monolayer TMDCs [17].

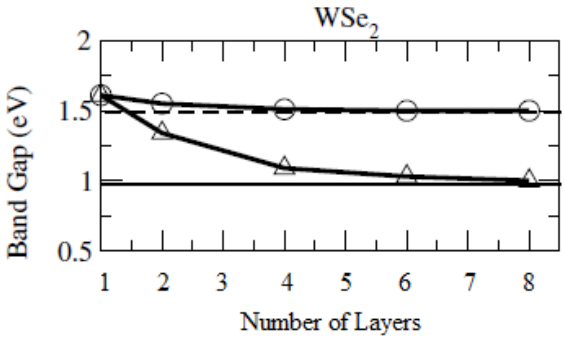

Figure 3.6 Variation of indirect band gap energies (solid lines with triangles) and direct band gap energies at the 'K' point (solid lines with circles) for WSe_2.

Source: Kumar, A., & Ahluwalia, P. K. (2012). Electronic structure of transition metal dichalcogenides monolayers 1H-MX2 (M= Mo, W; X= S, Se, Te) from ab-initio theory: new direct band gap semiconductors. The European Physical Journal B, 85(6), 1-7.

Figure 3.6 shows a variation of indirect band gap energies and direct band gap energies at the 'K' point. The horizontal dotted line and solid line indicate the direct gap at 'K' point and indirect gap respectively for bulk materials. As reported by Kumar et al [14], the indirect band gap energies in the bulk are blue-shifted relative to the direct band gap in the monolayer limit. This leads to the tunability of the electronic band gap [14].

3.4 Temperature Dependence of Energy Gap of Monolayer $MoSe_2$ and WSe_2

The energy gap of a semiconductor depends on temperature. In most semiconductors, the energy gap decreases with increase in temperature. There is an increase in atomic spacing due to increase in lattice vibrations because of an increase in thermal energy. Hence, an increased interatomic spacing decreases the potential seen by the electrons in the material, which in turn reduces the size of the energy gap [18].

The temperature dependence of the energy gap of $MoSe_2$ and WSe_2 were determined by using Equation (3.1). As formulated by O'Donnell, the equation serves to be a direct replacement of Varshini's equation [19].

$$E_g(T) = E_g(0) - S\langle\hbar\omega\rangle[(\coth\langle\hbar\omega\rangle / 2kT) - 1] \quad (3.1)$$

Here, $E_g(0)$ is the band gap at 0 K, S is a dimensionless coupling constant and $\langle\hbar\omega\rangle$ is an average phonon energy. This equation was found to have better fitting results compared to other theoretical approaches [18]. Fitting parameters, based on Equation (3.1), are shown in Table 3.1. Monolayer $MoSe_2$ and WSe_2 were considered in this study.

Table 3.1 Fitting parameters of E_g for monolayer $MoSe_2$ and WSe_2

Material	Eg (0) (eV)	S	$\langle\hbar\omega\rangle$ (meV)	References
$MoSe_2$	1.640	1.93	1.16	19
WSe_2	1.742	2.06	1.50	20

Figure 3.7 shows the variation of band gap with temperature while Figure 3.8 shows the dE_g/dt plot of monolayer $MoSe_2$ and WSe_2. As observed from Figure 3.7, the energy gap decreases with increase in temperature, which is generally the case for most semiconductors. Whereas, Figure 3.8 shows that the dEg/dT of both materials is non-linear with temperature and negative and decreases with increase in temperature.

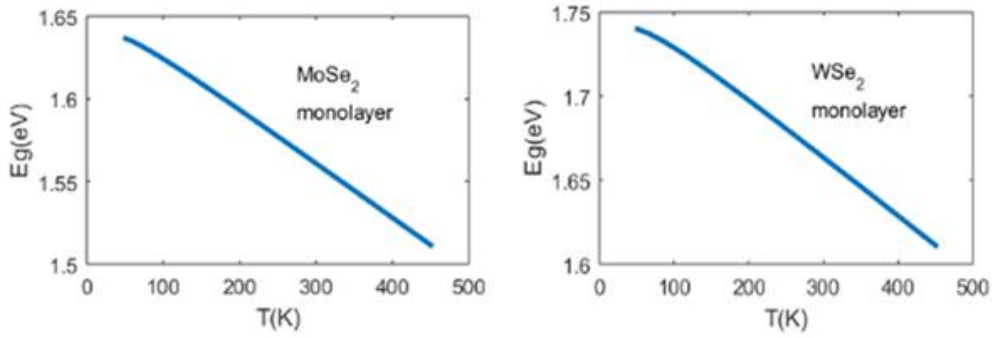

Figure 3.7 Temperature dependence curve of monolayer $MoSe_2$ and WSe_2.

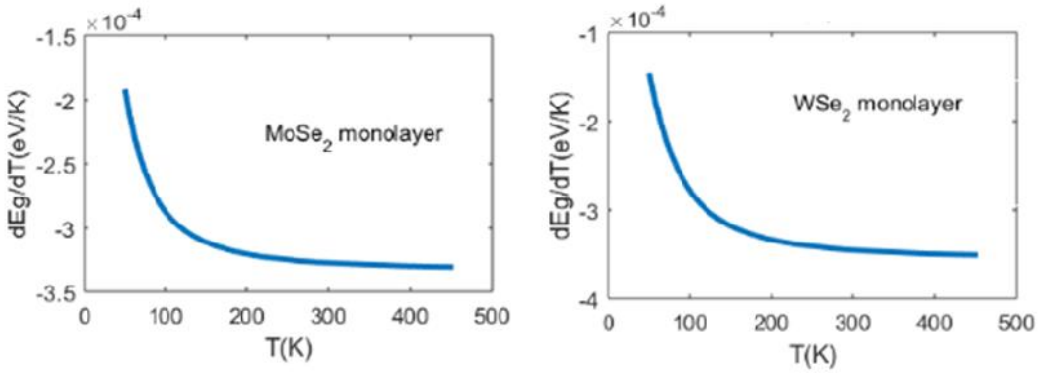

Figure 3.8 $\frac{dE_g}{dt}$ of monolayer $MoSe_2$ and WSe_2.

Investigation of the monolayer and bulk electronic structures of $MoSe_2$ and WSe_2, in this Chapter, provide an insight into the possible applications of these materials in the field of nanoelectronics. The large separation in valleys of K-space due to suppression of intervalley scattering could open the gates to a new field of electronics called valleytronics [20]. Band gap engineering is an important field in electronics; the ability to control the band gap of a semiconductor facilitates to create desirable electrical and optical properties. Surface doping can control the band structure of WSe_2; this control permits to alter the size of the gap and direct−indirect band gap transition [17].

CHAPTER 4

ELECTRICAL PROPERTIES OF $MoSe_2$ and WSe_2

The band gap analysis and temperature dependence study discussed in the earlier Chapter help to understand the semiconductor behavior of $MoSe_2$ and WSe_2 at a fundamental level. The band gap transitions at monolayer and bulk levels make them suitable candidates for applications in the semiconductor industry. This Chapter primarily focuses on the electrical transport properties of $MoSe_2$ and WSe_2, an in-depth literature survey of resistivity calculations performed and reported by various authors. Most of the electrical transport properties are observed at the monolayer level for these materials.

4.1 General Considerations

4.1.1 Sheet Resistance

Resistivity of a material is given by Equation (4.1),

$$\rho = \frac{1}{\sigma} = \frac{1}{q(n\,\mu_n + p\,\mu_p)} \tag{4.1}$$

The equation gives a relation between the resistivity and conductivity of a material and also displays that resisitivity is inversely related to the mobility of charge carriers i.e., electrons and holes. The resistivity hence depends on temperature and doping density of the material [18].

Sheet resistance is given by Equation (4.2), where 'R_s' is the sheet resisitance, 't' is the thickness of the wafer and 'ρ' is the resisitivity of a layer of the material. Sheet resisitance gives the resistance of the material across its given thickness.

$$R_s = \frac{\rho}{l} \tag{4.2}$$

The units of sheet resistance is Ohms, but in some cases it is also given by Ohms per square. This nomenclature comes in handy when the resistance of a rectangular piece of material with length, 'L', and width 'W' must be obtained. It equals the product of the sheet resistance and the number of squares and is give by Equation (4.3) [18].

$$R = R_s \frac{L}{W} \tag{4.3}$$

4.1.2 Electron Mobility

Electron mobility characterizes how quickly an electron travels through a metal or a semiconductor under the influence of an electric field. Carrier mobility is used to denote the charge carriers of a material i.e., electrons and holes. Equation (4.4) gives the general equation of electron mobilty (denoted by μ).

$$\mu = \frac{v_d}{E} \tag{4.4}$$

'v_d' is the drift velocity and 'E' is the electric field applied across a piece of material [18].

Mobility of charge carriers or carrier mobility plays a very important role in determining the electrical property of a material. This mobility depends on the number of

charge carriers and doping concentration in a material. Equation (4.5) denotes the mobility at a particular doping density at room temperature.

$$\mu = \mu_{min} + \frac{\mu_{max} - \mu_{min}}{1+(\frac{N^{\alpha}}{N_r})} \quad (4.5)$$

Where, μ_{min}, μ_{max}, α and N_r are fitting parameters and N is the doping density [18].

4.1.3 Hall Effect and Hall Coefficient

Hall effect helps us understand the behavior of free charge carriers in a semiconductor under the influence of applied electric and magnetic fields. Figure 4.1 shows a semiconductor bar with a rectangular cross section and length 'L'. A voltage 'V_x' is applied between the two contacts, resulting in a field 'E_x' along the x-direction. The magnetic field 'B_z' is applied in the z-direction.

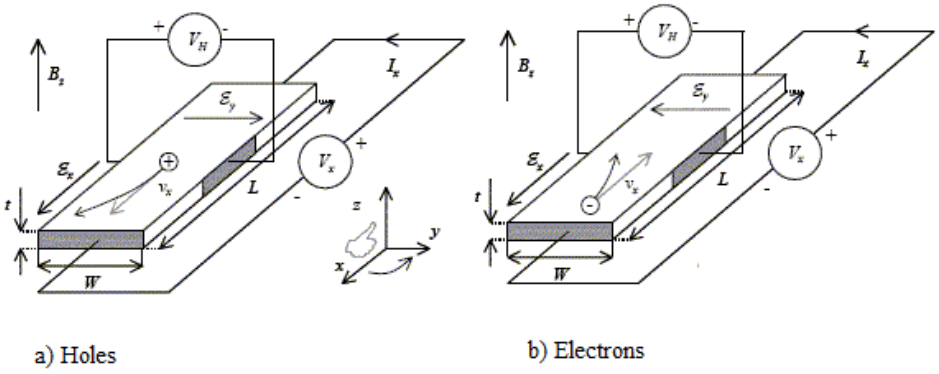

Figure 4.1 Hall setup and carrier motion for a) Holes and b) Electrons.

Source : Van Zeghbroeck, B. (2011). Principles of electronic devices. University of Colorado.

As seen from Figure 4.1 (a), the holes move in the positive x-direction. The magnetic field causes a force 'F_y' to act on the mobile particles in a direction according to the right hand rule [18]. As a result, there is a force, 'F_y', along the positive y-direction, which moves the holes to the right. In steady state this force is balanced by an electric field, 'y', so that there is no net force on the holes. As a result, there is a voltage across the sample, which can be measured with a high-impedance voltmeter. This voltage, 'V_H', is called the Hall voltage [18].

Figure 4.1 (b) shows the behavior of electrons. The electrons travel in the negative x-direction. Therefore, the force, 'F_y', is in the positive y-direction due to the negative charge and the electrons move to the right, just like holes. The balancing electric field, 'y', now has the opposite sign, which results in a negative Hall voltage [18].

Equation (4.6) gives the Hall field (E_y),

$$E_y = v_x B_z = \frac{J_x}{q p_{p^0}} B_z \tag{4.6}$$

The Hall coefficient, 'R_H', is defined as the Hall field divided by the current density, 'J_x', and magnetic field, 'B_z' and is given by Equation (4.7).

$$R_H = \frac{Ey}{J_x B_z} = \frac{1}{q p_{p^0}} \tag{4.7}$$

A measurement of the Hall voltage is often used to determine the type of semiconductor (n-type or p-type) the free carrier density and the carrier mobility. Since the measurement can be done on a small piece of uniformly doped material, it is by far the easiest measurement to determine the carrier mobility [18].

4.2 Case Study of Electrical Properties of $MoSe_2$ and WSe_2

The electrical properties such as electron mobility, hall effect, hall coefficient, sheet resistance etc. are a build up to the similar properties observed in $MoSe_2$ and WSe_2. This section complies experimental results and computational methods discussed in various literature. Brumme et al. [21], presented a study of structural, electronic, and transport properties of $MoSe_2$ and WSe_2 and also examined these properties under field-effect doping for $MoSe_2$ and WSe_2 [21]. By using a theoretical approach to simulate and model the doping in field-effect devices, Brumma et al applied this approach to the H polytypes of $MoSe_2$ and WSe_2 apart from other TMDCs discussed in the literature [21].

4.2.1 Effect of Doping

A FET setup is modeled to analyze the quantum capacitance and effect of doping on the band structure and electrical properties of TMDCs. Figure 4.2 depicts this FET structure and includes the equilvalent circuit for overall capacitance seen at the gate electrode.

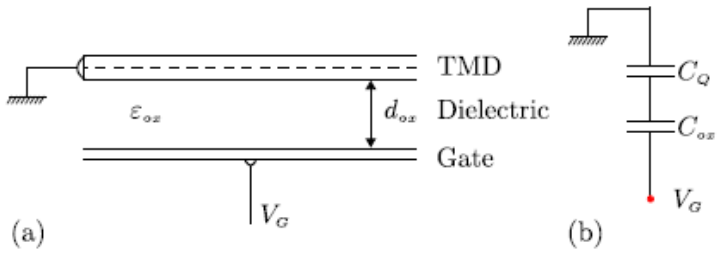

Figure 4.2 Schematic illustration of an FET setup in which the 2D metallic system is separated from the gate electrode by a dielectric with dielectric constant ε_{ox} of thickness d_{ox}. (b) Equivalent circuit for the overall capacitance seen at the gate electrode.

Source: Brumme, T., Calandra, M., & Mauri, F. (2015). First-principles theory of field-effect doping in transition-metal dichalcogenides: Structural properties, electronic structure, Hall coefficient, and electrical conductivity. Physical Review B, 91(15), 155436.

Doping was done via the FET setup and had a minor influence on the structure of $MoSe_2$ and WSe_2. Weak polarity of the bonds between the transition metal atom and chalcogen atom account for the minor influence on the structure [21]. The largest change was found out for the layer thickness of the layer closest to the charged plane representing the gate electrode [21]. The layer thickness increased by ≈ 0.06 Å for a large electron doping of n = −0.3 e/unit cell ($n \approx -3.16 \times 10^{14}$ cm^{-2}) and decreased by ≈ 0.02 Å for a large hole doping of n = +0.3 e/unit cell. This change was mainly due to the increase/decrease of the chalcogen–transition-metal bond length of those being closest to the gate. Bonds lengths of ≈ +0.04 Å for n = −0.3 e/unit cell and ≈ −0.02 Å for n = +0.3 e/unit cell were reported. Accordingly, there was also a small change in the angle between the first chalcogen, the transition metal, and the second chalcogen of up to +0.9° (−0.4°) for large electron/hole doping [21].

4.2.2 Hall Effect Measurements

A hall experiment is generally carried out to determine the doping charge in a sample. The inverse Hall coefficient is directly proportional to the charge-carrier density n in the case of parabolic, isotropic bands [21]. The hall coefficient calculations were carried out within the Boltzmann transport theory. Equations of hall coefficient, current density, conductivity distribution and charge doping concentrations were formulated by considering a 3D system. After expressing the conductivity tensor equations at a given temperature 'T' and chemical potential 'E_f', within the relaxation-time approximation, followed by assuming quadratic dispersion of bands to formulate a dispersion relation for a quadratic, isotropic

band in two dimensions. Finally, the equation for hall coefficient was developed assuming conditions of normal magnetic field [21].

$$R_{xyz}(0; E_f) = \frac{\sum_i m_i^{-2} n_i}{q(\sum_i m_i^{-1} n_i)^2} . \quad (4.8)$$

In Equation (4.8), 'm_i' is the valley-independent effective mass and 'n_i' is the doping-charge constant. The conductivity in two dimensions is independent of the mass of the charge carriers, since the density 'n' is proportional to 'm'. The Hall coefficient is inversely proportional to the mass 'm' in the 2D case. Equation (4.8) is only valid as long as there are only bands with isotropic, quadratic dispersion and if $\tau_{i,k} = \tau (E_F)$, where τ is relaxation time dependent on band index (i) and k-vector direction [21].

Figure 4.3 shows the ratio of inverse hall coefficient to the doping charge concentration as a function of doping for the monolayer $MoSe_2$ and WSe_2 materials. A comparison between curves at T = 0 K and T = 300 K is also shown. We understand that temperature has a minor influence on the inverse Hall coefficient for $MoSe_2$ and WSe_2. It is interesting to note that a peak is observed at $n \approx 0.1$ e/unit cell for both materials. However, the inverse hall coefficient of monolayer $MoSe_2$ was found to be slightly higher than that of monolayer WSe_2. The doping-charge concentration calculated using the inverse Hall coefficient was reported to be 1.5 times larger than the real concentration. The deviation of the inverse Hall coefficient from the doping charge n increases with increasing doping of the valence-band maximum at K [21].

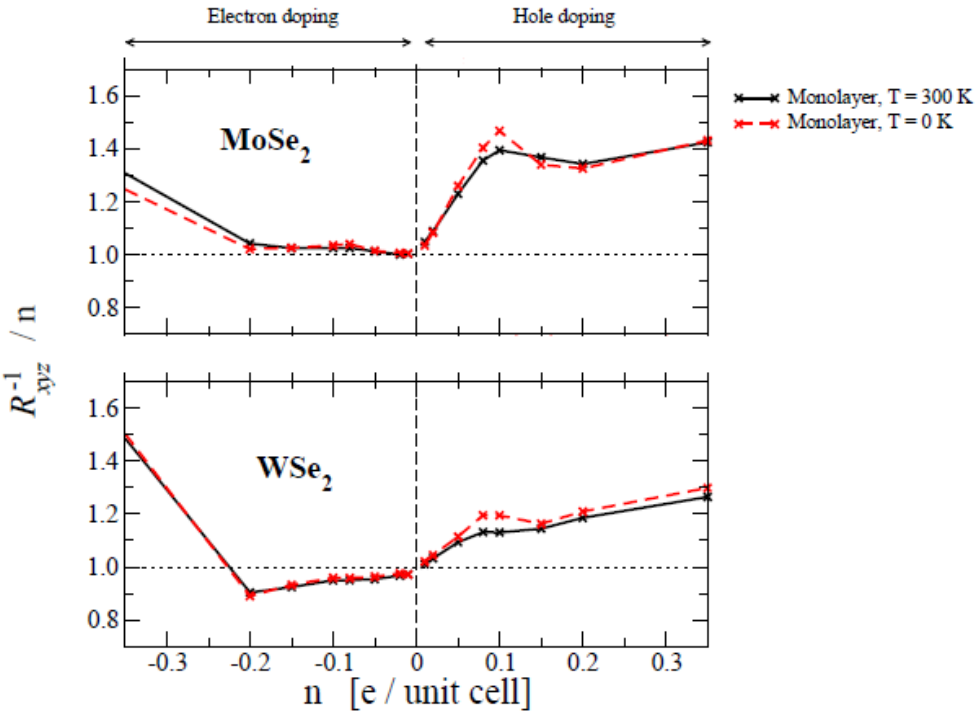

Figure 4.3 Ratio of the inverse Hall coefficient to the doping charge as function of doping for monolayer $MoSe_2$ and WSe_2 at temperatures T = 0 K and T = 300 K.

Source: Brumme, T., Calandra, M., & Mauri, F. (2015). First-principles theory of field-effect doping in transition-metal dichalcogenides: Structural properties, electronic structure, Hall coefficient, and electrical conductivity. Physical Review B, 91(15), 155436.

Figure 4.4 Shows the ratio of the inverse Hall coefficient to the doping charge as a function of doping for monolayer, bilayer and trilayers of $MoSe_2$ and WSe_2 at a temperature of T = 300 K. As observed from the figure, Monolayer $MoSe_2$ and WSe_2 have higher inverse Hall coefficient at same levels of hole doping concentrations i.e., $n \approx +1.4 \times 10^{14}$ cm^{-2} when compared to different levels of layer thicknesses. Monolayer $MoSe_2$ has a higher inverse hall coefficient compared to monolayer WSe_2.

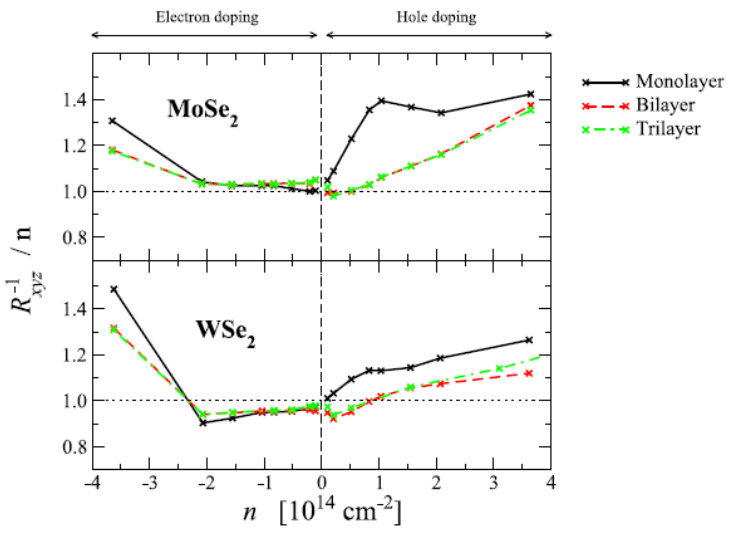

Figure 4.4 Ratio of the inverse Hall coefficient to the doping charge as a function of doping for monolayer, bilayer and trilayers of $MoSe_2$ and WSe_2 at a temperature of T = 300 K.

Source: Brumme, T., Calandra, M., & Mauri, F. (2015). First-principles theory of field-effect doping in transition-metal dichalcogenides: Structural properties, electronic structure, Hall coefficient, and electrical conductivity. Physical Review B, 91(15), 155436.

4.2.3 Resistivity Measurements

Resistivity of a material depends on the temperature, area and its thickness. The relation is given by Equation (4.9),

$$\rho = R\frac{A}{t} \tag{4.9}$$

Where, 'ρ' is the resistivity of the material, 'R' is the resistance of the material, 'A' is the area of the material and 't' is the thickness of the material.

Thakar et al. [22] presented the variation of resistivity with temperature for $MoSe_2$ and WSe_2 crystals. It is safe to assume that the thickness of crystals were at the bulk level and nowhere near the monolayer level [22]. These investigations were carried out for resistivity along the C axis. Figure 4.5 shows the variation of resistance with temperature

along the C axis for $MoSe_2$ and WSe_2 crystals; While Figure 4.6 shows the variation of resistivity with temperature along the C axis for $MoSe_2$ and WSe_2 crystals.

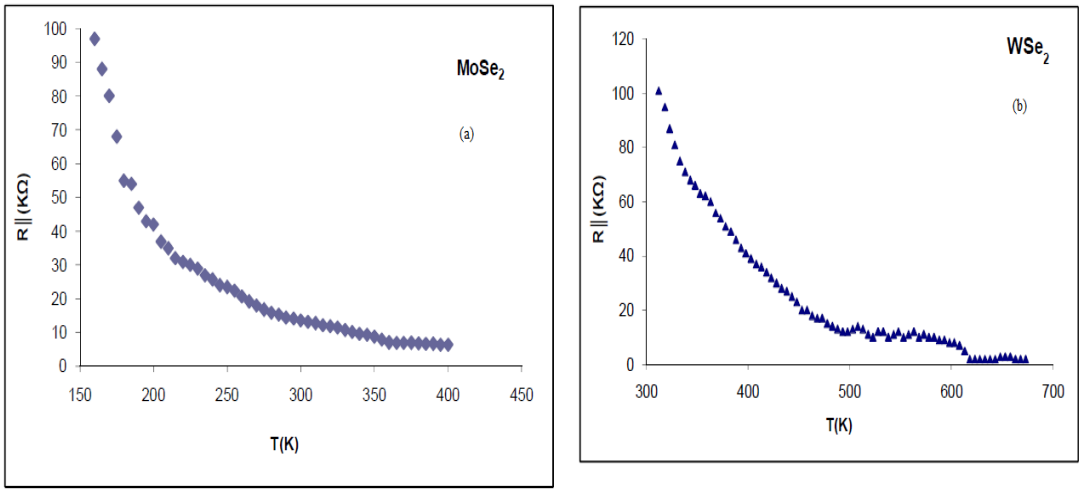

Figure 4.5 Variation of resistance (along c axis) with temperature of (a) $MoSe_2$ crystal and (b) WSe_2 crystal.

Source: Thakar, Bhavesh Amrutbhai. Investigations of TMDCs and use in solar cell. Thesis. Hemchandracharya North Gujarat University, Patan, 2011. Shodhganga. Web. 23-Jun-2015. < http://shodhganga.inflibnet.ac.in/handle/10603/43941>

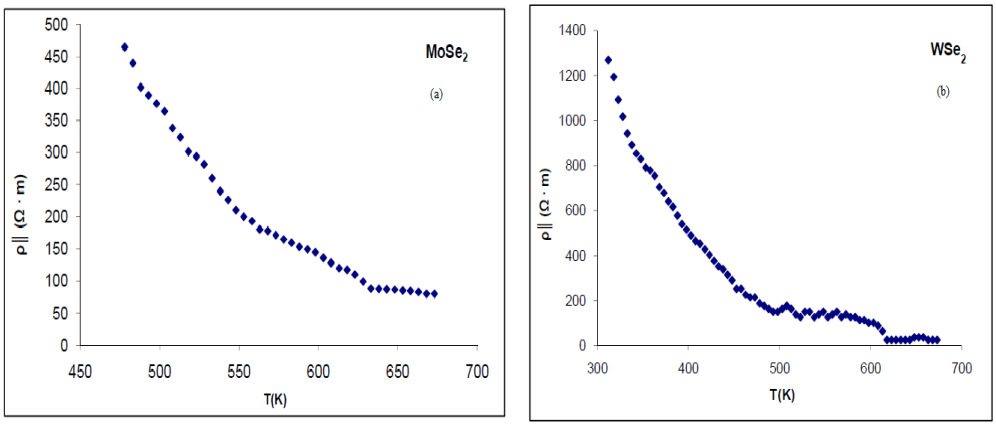

Figure 4.6 Variation of resistivity (along c axis) with temperature of (a) $MoSe_2$ crystal and (b) WSe_2 crystal.

Source: Thakar, Bhavesh Amrutbhai. Investigations of TMDCs and use in solar cell. Thesis. Hemchandracharya North Gujarat University, Patan, 2011. Shodhganga. Web. 23-Jun-2015. < http://shodhganga.inflibnet.ac.in/handle/10603/43941>

As seen from Figures 4.5 and 4.6, the resistance and resistivity of $MoSe_2$ and WSe_2 crystals decrease exponentialy with increase in temperature. Figure 4.7 shows the variation of resistance with temperature perpendicular the C axis for $MoSe_2$ and WSe_2 crystals, While Figure 4.8 shows the variation of resistivity with temperature perpendicular the C axis for $MoSe_2$ and WSe_2 crystals.

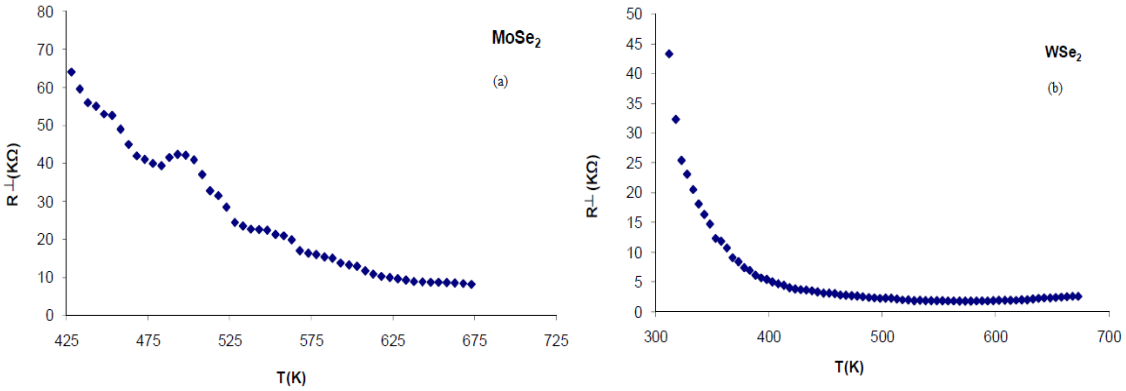

Figure 4.7 Variation of resistance (perpendicular to c axis) with temperature of the (a) $MoSe_2$ crystal (b) WSe_2 crystal.

Source: Thakar, Bhavesh Amrutbhai. Investigations of TMDCs and use in solar cell. Thesis. Hemchandracharya North Gujarat University, Patan, 2011. Shodhganga. Web. 23-Jun-2015. < http://shodhganga.inflibnet.ac.in/handle/10603/43941>

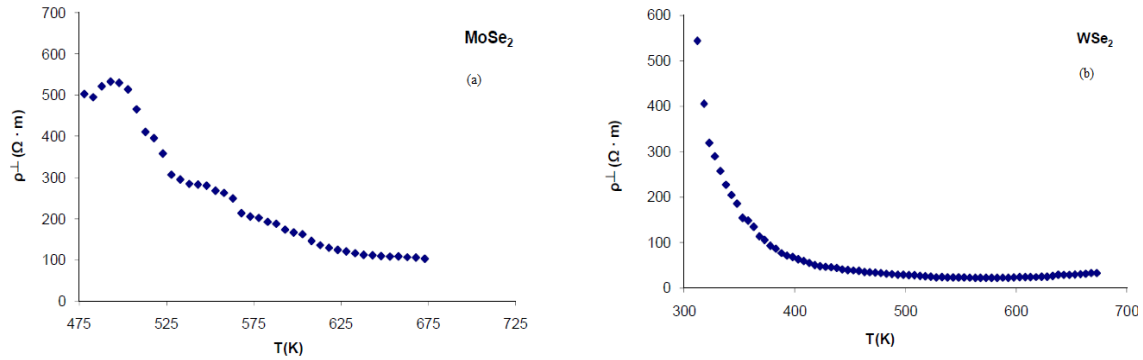

Figure 4.8 Variation of resistivity (perpendicular to c axis) with temperature of the (a) $MoSe_2$ crystal (b) WSe_2 crystal.

Source: Thakar, Bhavesh Amrutbhai. Investigations of TMDCs and use in solar cell. Thesis. Hemchandracharya North Gujarat University, Patan, 2011. Shodhganga. Web. 23-Jun-2015. < http://shodhganga.inflibnet.ac.in/handle/10603/43941>

While comparing the resistivity plots of Figures 4.6 and 4.8 we find that the resistivity plot parallel to c axis is much higher than the one compared to resistivity plot for perpendicular to c axis. This trend was seen due to the layered structure of the crystals [22].

Electrical properties of $MoSe_2$ and WSe_2 were touched upon in this section of the thesis. However, these are case studies which help us understand the semiconductor nature of these materials at different temperatures and varying thicknesses. Most of the research on electrical properties of these materials are application based, i.e., Applications of these materials in Field Effect Transistors.

CHAPTER 5

OPTICAL PROPERTIES OF $MoSe_2$ and WSe_2

$MoSe_2$ and WSe_2 are direct band gap semiconductors at monolayer level and indirect band gap semiconductors at bulk level. The band gaps of these materials are in the visible region of the spectra (400 nm – 700 nm). In recent years, there has been a large volume of research conducted on the optical properties of TMDCs. However, much of the research revolves around the spectral reflectance, differential reflectance, differential transmittance, spectral absorptance and absorbance. These studies are usually based on experimental research and very less or, in some cases, no simulations are carried out. Despite the intense research carried out on the optical properties of TMDCs, none of the studies gives a definite value of refractive indices and extinction coefficients. Furthermore, the results of most of the studies involving reflectance, absorptance and transmittance calculations are not in accordance with each other and there is a large spread in the obtained data of the optical properties.

In this work, the values of optical constants (n and k) and optical properties (R, T and A) are determined by using the MATLAB software under conditions of normal incidence and room temperature. Li et al. [23] have reported their studies of the dielectric constants for monolayer $MoSe_2$ and WSe_2 at room temperature (ε_1 and ε_2) from experimental reflectance spectra by a constrained Kramers-Kronig analysis. These values were used to calculate the photon energy-dependent refractive index and extinction coefficient. As reported by Mukherjee et al. [24], the values determined by Li et al. [23]

were found to be better than the set of values determined by other authors and hence were chosen to analyze the optical properties.

5.1 Mathematical Modeling

The refractive index (n) and extinction coefficient (k) of a material are related to the complex dielectric constants 'ε_1' and 'ε_2'. The complex dielectric function ($\varepsilon_r = \varepsilon_1 + i\varepsilon_2$) is a function of the amount of light absorbed by the material. The complex dielectric constants are related to the optical constants by the following set of equations.

$$\varepsilon_1 = n^2 - k^2 \tag{5.1}$$

$$\varepsilon_2 = 2nk \tag{5.2}$$

Here, 'n' and 'k' are the refractive index and extinction coefficient of the material, respectively.

From Equations (5.1) and (5.2), we get:

$$4n^4 - 4n^2\,\varepsilon_1 - \varepsilon_2^2 \tag{5.3}$$

$$k = \frac{\varepsilon 2}{2n} \tag{5.4}$$

By solving Equation (5.3), multiple values of 'n' were found; the real and positive values of 'n' were chosen to get the values of extinction coefficient 'k' from Equation (5.4).

The next set of equations were used to obtain the optical properties of monolayer and bulk $MoSe_2$ and WSe_2 between the energy ranges of 1.5 eV – 3.0 eV. Under conditions

of normal incidence, Reflectance (R), Transmittance (T) and Absorptance (A) are given by:

$$R = \frac{(n-1)^2+k^2}{(n+1)^2+k^2} \tag{5.5}$$

$$T = (1\text{-}R)\,(e^{-\alpha t}) \tag{5.6}$$

In Equation (5.6), 't' is the layer thickness and 'α' is the absorption coefficient.

$$\alpha = \frac{4\pi k}{\lambda} \tag{5.7}$$

Here, 'k' is the extinction coefficient of the TMDC and 'λ' is the wavelength (in nm) of the photon incident on the TMDC material.

$$A = 1 - R - T \tag{5.8}$$

The above calculations were performed for suspended monolayer, bulk $MoSe_2$ and WSe_2, and are dependent on the incident photon energy and thickness of the material. Equation (5.9) was used to compute the optical properties of $MoSe_2$ and WSe_2 on various substrates.

$$R = \frac{(n_1-n_2)^2+k_1^2}{(n_1+n_2)^2+k_1^2} \tag{5.9}$$

Here, 'n_1' and 'k_1' are the refractive index and extinction coefficient of the TMDC, respectively, and 'n_2' is the refractive index of the substrate. The transmittance and absorptance calculations for double layer follow the conventional phenomenological approach. The interface at the double layer is considered to be abrupt (no mixing or roughness at the interface is considered in these calculations).

5.2 Optical Constants of $MoSe_2$ and WSe_2

The optical constants of $MoSe_2$ and WSe_2 were simulated using the MATLAB software. Figure 5.1 shows the 'ε_1' and 'ε_2' values reported by Li et al. [23] and which were used to obtain the values of 'n' and 'k' in this work. Monolayer thickness of $MoSe_2$ and WSe_2 were taken as 0.70 nm [6], whereas, bulk thickness of $MoSe_2$ and WSe_2 were taken as 20 nm, which seemed to be the optimal value for the TMDCs [4].

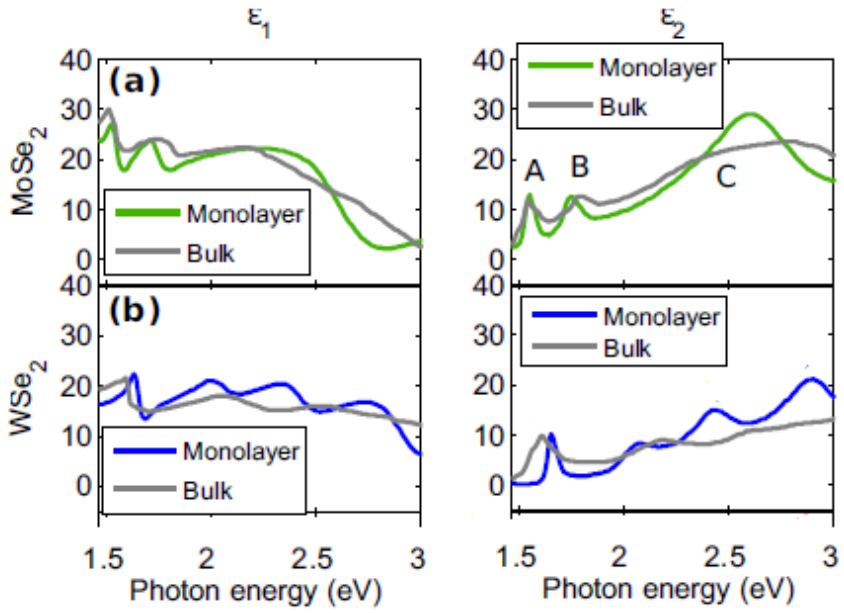

Figure 5.1 Dielectric functions of monolayer and bulk $MoSe_2$ and WSe_2.

Source: Li, Y., Chernikov, A., Zhang, X., Rigosi, A., Hill, H. M., van der Zande, A. M., & Heinz, T. F. (2014). Measurement of the optical dielectric function of monolayer transition-metal dichalcogenides: MoS_2, $MoSe_2$, WS_2, and WSe_2. Physical Review B, 90(20), 205422.

Figures 5.2 and 5.3 show the simulated values of ‘n’ and ‘k’ for monolayer and bulk $MoSe_2$ and WSe_2.

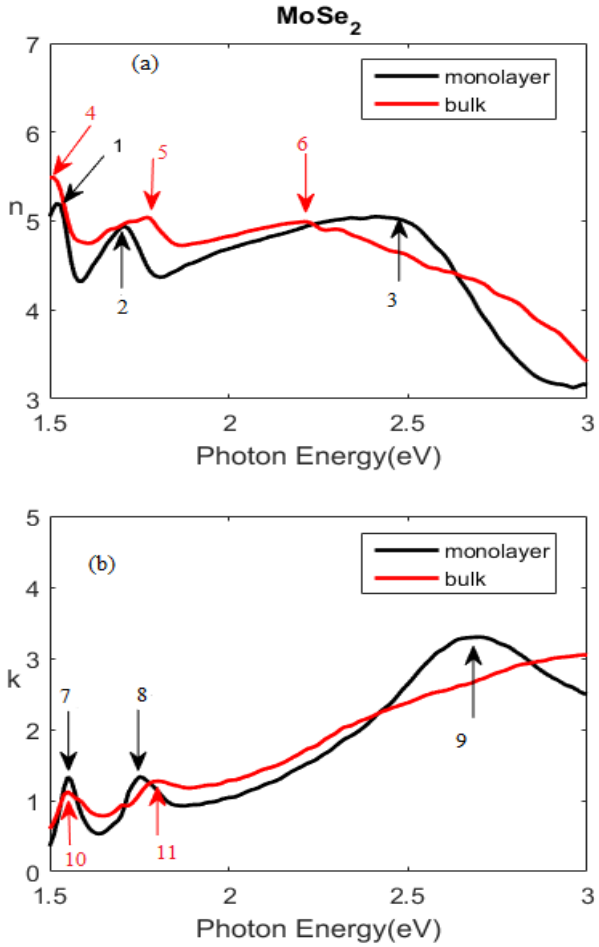

Figure 5.2 Refractive index and extinction coefficient as a function of photon energy for suspended monolayer and bulk $MoSe_2$.

The maximum value of refractive index (n) and the corresponding energy (E) for monolayer $MoSe_2$ is 5.20 (1.52 eV) and for bulk $MoSe_2$ is 5.49 (1.51 eV). Whereas, the maximum value of extinction coefficient (k) and the corresponding energy (E) for monolayer $MoSe_2$ is 3.29 (2.70 eV) and for bulk $MoSe_2$ is 2.42 (3.00 eV).

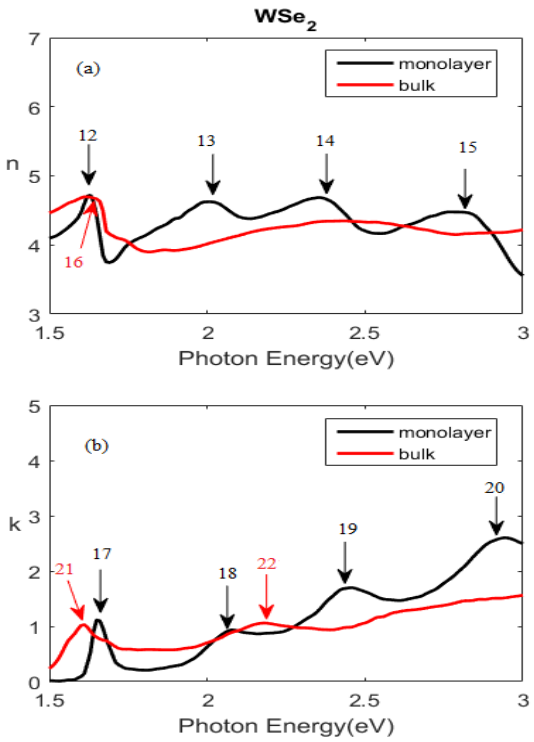

Figure 5.3 Refractive index and extinction coefficient as a function of photon energy for suspended monolayer and bulk WSe_2.

The maximum value of refractive index (n) and the corresponding energy (E) for monolayer WSe_2 is 4.72 (1.63 eV) and for bulk WSe_2 is 4.69 (1.62 eV). Whereas, the maximum value of extinction coefficient (k) and the corresponding energy (E) for monolayer WSe_2 is 2.60 (2.94 eV) and for bulk WSe_2 is 1.56 (3.00 eV).

The difference in the maximum values of n between monolayer and bulk is significant and hence we can conclude that a change in the thickness of the material does affect the refractive index. A similar trend is observed for extinction coefficient values and hence we conclude that thickness of the material affects the extinction coefficient also. These values are in agreement with the values reported by Zhang et al. [25] and are very close to the values presented by Liu et al. [26]. In addition, the energies corresponding to the maximum refractive index differ significantly between the bulk and the monolayer

levels. It should be noted that the above analysis is based on the range of photon energies, 1.5 to 3.0 eV, considered in this study. The energies corresponding to the features in the variations of n and k, with energy, for monolayer and bulk $MoSe_2$ and WSe_2 are summarized in Table 5.1.

Table 5.1 Energies Corresponding to Features of n (E) and k (E) for Suspended TMDCs.

Material	No.	E (eV)	n	No.	E (eV)	k
$MoSe_2$	1	1.52	5.20	7	1.55	1.33
monolayer	2	1.71	4.94	8	1.75	1.33
	3	2.41	5.05	9	2.70	3.30
$MoSe_2$ bulk	4	1.51	5.49	10	1.55	1.12
	5	1.77	5.04	11	1.80	1.27
	6	2.21	4.99			
WSe_2	12	1.63	4.72	17	1.65	1.12
monolayer	13	2.10	4.47	18	2.08	0.94
	14	2.36	4.68	19	2.46	1.69
	15	2.77	4.69	20	2.94	2.60
WSe_2 bulk	16	1.63	4.73	21	1.61	1.03
				22	2.18	1.06

5.3 Optical Properties of Suspended Monolayer and Bulk $MoSe_2$ and WSe_2

This section of the chapter focuses on the simulation of optical properties such as; Reflectance, Transmittance and Absorptance of suspended monolayer and bulk $MoSe_2$ and WSe_2 materials.

Figures 5.4 and 5.5 show the simulated R, T and A of suspended monolayer and bulk $MoSe_2$ and WSe_2 at room temperature and normal incidence. Absorptance spectra of monolayer and bulk are separated due to the large change in magnitude of absorptance of monolayer and bulk. This change is reasonable due to the increase in the number of layers which leads to increase in absorptance of light by the material. For materials, the two lowest energy peaks in the reflectance spectra correspond to the excitonic features associated with inter-band transitions in the K (K') point in the Brillouin zone [2]. The two significant peaks in Figure 5.4 can be attributed to the splitting of the valence bands by spin-orbit coupling [27]. At higher photon energies, a spectrally broad response is observed from higher-lying inter-band transitions, including the transitions near the Γ point [2].

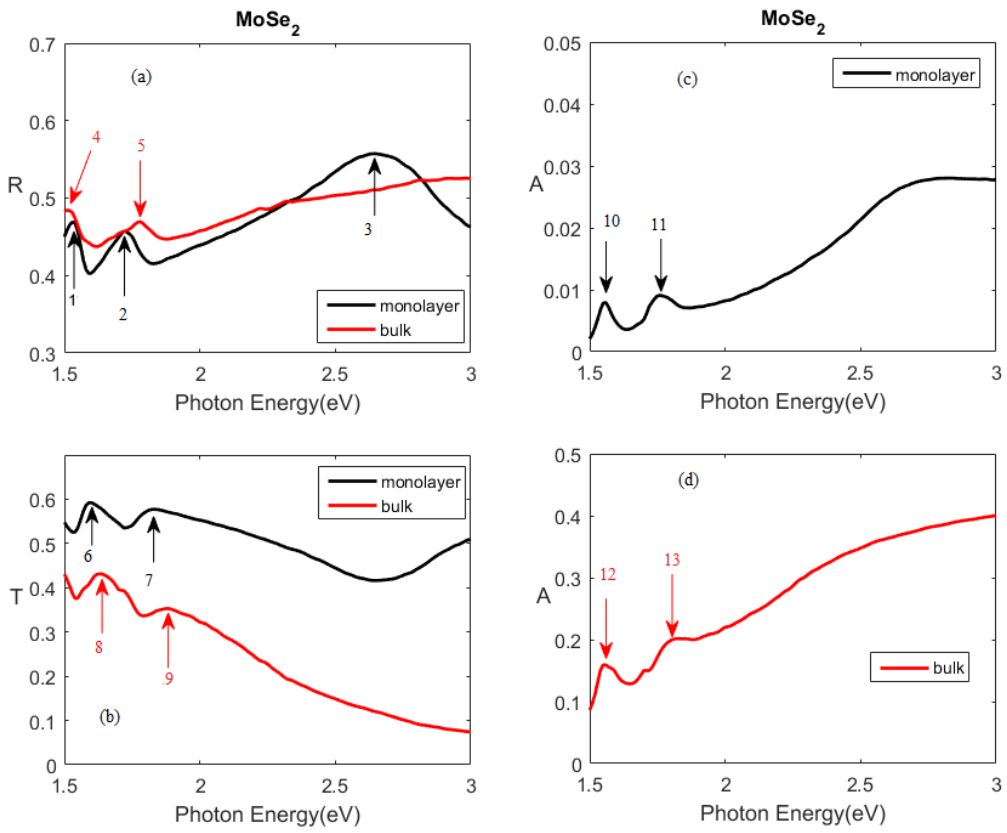

Figure 5.4 Simulated R, T and A of suspended monolayer and bulk $MoSe_2$.

The maximum value of Reflectance (R) and the corresponding energy (E) for monolayer $MoSe_2$ is 55.7% (2.64 eV). Similarly, the maximum value of (R) for bulk $MoSe_2$ is 52.6% (2.98 eV). The maximum value of Transmittance (T) and the corresponding energy (E) for monolayer $MoSe_2$ is 59.2% (1.60 eV). Similarly, the maximum value of (T) for bulk $MoSe_2$ is 43.1% (1.63 eV). The maximum value of Absorptance (A) and the corresponding energy (E) for monolayer $MoSe_2$ is 2.78%. Similarly, the maximum value of (A) for bulk $MoSe_2$ is 40.00%. From Figures 5.4 (c) and 5.4 (d) we observe that the location of peaks in either case remains relatively similar; these peaks are the A and B

exciton absorption peaks, which originate from the spin-split direct gap transitions at the K point of the Brillouin zone.

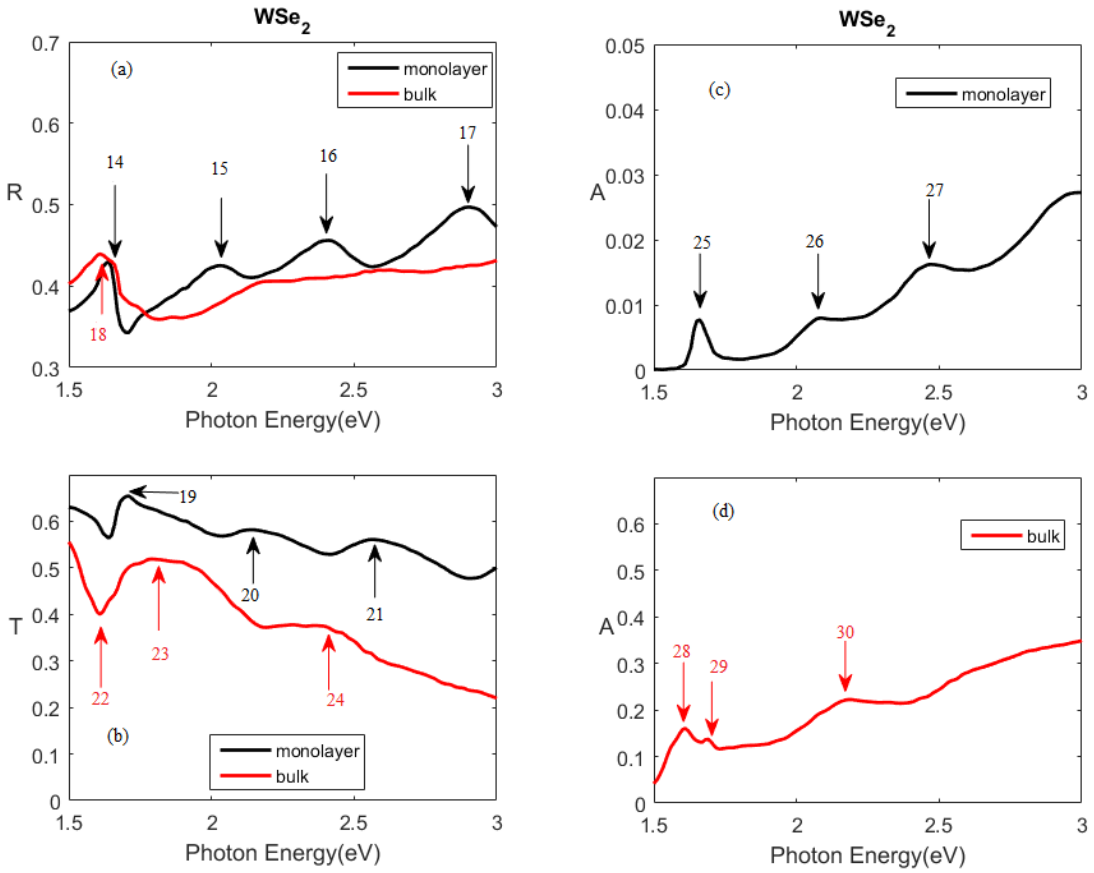

Figure 5.5 Simulated R, T and A for suspended monolayer and bulk WSe_2.

The maximum value of Reflectance (R) and the corresponding energy (E) for monolayer WSe_2 is 49.7% (2.90 eV). Similarly, the maximum value of (R) for bulk WSe_2 is 43.9% (1.61 eV). The maximum value of Transmittance (T) and the corresponding energy (E) for monolayer WSe_2 is 65.4% (1.71 eV). Similarly, the maximum value of (T) for bulk WSe_2 is 51.9% (1.79 eV). The maximum value of Absorptance (A) and the corresponding energy (E) for monolayer WSe_2 is 1.62% (2.47 eV). Similarly, the maximum value of (A) for bulk WSe_2 is 22.2% (2.19 eV). All the energy values

corresponding to the features, present in Figure 5.4 and Figure 5.5, are summarized in Table 5.2.

Table 5.2 Energies Corresponding to Features of R, T and A for Suspended TMDCs.

Material	No.	E (eV)	R	No.	E (eV)	T	No.	E (eV)	A
$MoSe_2$	1	1.53	0.469	6	1.60	0.592	10	1.56	0.00792
monolayer	2	1.72	0.457	7	1.83	0.577	11	1.76	0.00911
	3	2.64	0.557						
$MoSe_2$	4	1.51	0.484	8	1.63	0.432	12	1.55	0.159
bulk	5	1.78	0.469	9	1.88	0.353	13	1.82	0.202
WSe_2	14	1.64	0.430	19	1.71	0.654	25	1.66	0.00773
monolayer	15	2.03	0.425	20	2.14	0.582	26	2.09	0.00798
	16	2.41	0.456	21	2.56	0.561	27	2.47	0.01620
	17	2.90	0.497						
WSe_2	18	1.61	0.439	22	1.61	0.400	28	1.61	0.160
bulk				23	1.79	0.519	29	1.69	0.137
				24	2.29	0.378	30	2.19	0.222

5.4 Optical Properties of Monolayer, Bulk $MoSe_2$, and WSe_2 on Various Substrates.

In recent years, large volume of research is being done on the applications of TMDCs as heterojunction and heterostructure devices. By exploring the optical properties of these materials on various substrates such as gold, silicon and fused silica, a potential application

of these materials as contact semiconductors has been established. In this study, the thickness of silicon and fused silica substrate was assumed ~ 650 µm and thickness of gold substrate was assumed ~ 10 µm while performing all simulations.

5.4.1 Optical Properties of TMDCs on Gold Substrate

Figure 5.6 shows the shows the simulated reflectance and absorptance spectra of monolayer and bulk $MoSe_2$ and WSe_2 on a gold substrate.

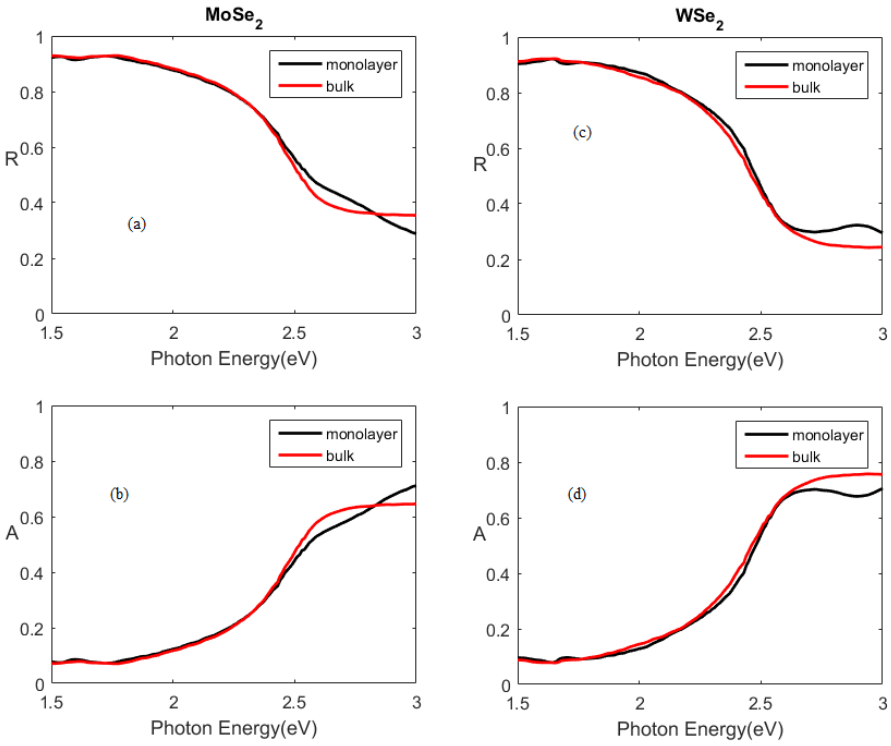

Figure 5.6 Simulated reflectance and absorptance spectra of monolayer and bulk TMDCs/Au.

It is observed that the reflectance tends to decrease with increase in photon energy, while the absorptance of increases with the increase in photon energy. Due to the large

thickness of gold considered in the simulations, the transmittance of these multilayers is ~0 in this energy range; thus reflectance and absorptance are complementary with each other.

As observed in the figures, the change in thickness of TMDC does not necessarily cause a significant change in the reflectance and absorptance of the TMDC/Au. No sharp peaks were observed in the reflectance and absorptance spectra. Maximum values of reflectance and absorptance for monolayer TMDC/Au and bulk TMDC/Au remained approximately the same, with maximum reflectance of ~90% and maximum absorptance of ~70%. It is to be noted within this context that, for the wavelength range considered in this study, the transmittance of gold is ~0 for film thickness of 0.1 microns.

5.4.2 Optical Properties of TMDCs on Silicon Substrate

Figure 5.7 shows the simulated reflectance and absorptance spectra of monolayer and bulk $MoSe_2$ and WSe_2 on a silicon substrate.

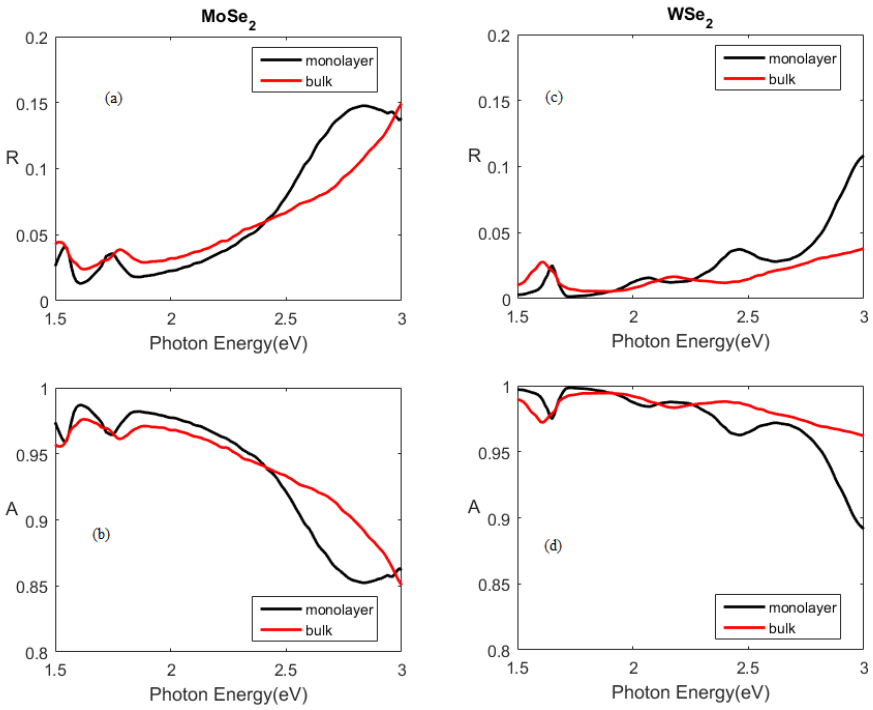

Figure 5.7 Simulated reflectance and absorptance spectra of monolayer and bulk TMDCs/Si.

As observed from Figure 5.7, the maximum values of Reflectance (R) for monolayer $MoSe_2$ and WSe_2 on silicon are, as follows: 14.76% (2.84 eV) and 10.84%, respectively. Similarly, the maximum value of (R) for bulk $MoSe_2$ and WSe_2 on silicon are 14.94% and 3.80%, respectively. Unless otherwise specified, the maximum values occur at 3 eV. The maximum value of Absorptance (A) for monolayer $MoSe_2$ and WSe_2 on silicon are as follows: 98.2% (1.61 eV) and 99.84% (1.73 eV), respectively. The maximum value of A for bulk $MoSe_2$ and WSe_2 on silicon are 97.6% (1.62 eV) and 99.44% (1.90 eV), respectively. Unless otherwise specified, the maximum values occur at 1.5 eV. The average maximum value of reflectance has a very low value as compared to that of TMDC/Au. The absorptance of TMDC/Si is very high compared to that of TMDC/Au.

Similar to TMDC/Au, the transmittance of TMDC/Si is ~ 0 due to the large thickness of the silicon wafer and is therefore not included in this study.

5.4.3 Optical Properties of TMDCs on Fused Silica Substrate

Figures 5.8 and 5.9 show the simulated reflectance, transmittance and absorptance spectra of monolayer and bulk $MoSe_2$ and WSe_2 on a fused silica substrate.

It is observed that the transmittance of TMDC/Fused Silica is substantially high which could be attributed to the transparency of fused silica and TMDCs. As observed from Figure 5.8, the maximum value of Reflectance (R) for monolayer $MoSe_2$ and WSe_2 on fused silica are as follows: 42.74% (2.65 eV) and 35.94% (2.90 eV), respectively. The maximum value of (R) for bulk $MoSe_2$ and WSe_2 on fused silica are 39.41% (3.00 eV) and 29.76% (1.61 eV), respectively. The maximum value of Transmittance (T) for monolayer $MoSe_2$ and WSe_2 on fused silica are, respectively, as follows: 73.37% (1.60 eV) and 80.26% (2.07 eV). The maximum value of 'T' for bulk $MoSe_2$ and WSe_2 on fused silica at 1.50 eV, are 54.75%, and 68.86%, respectively.

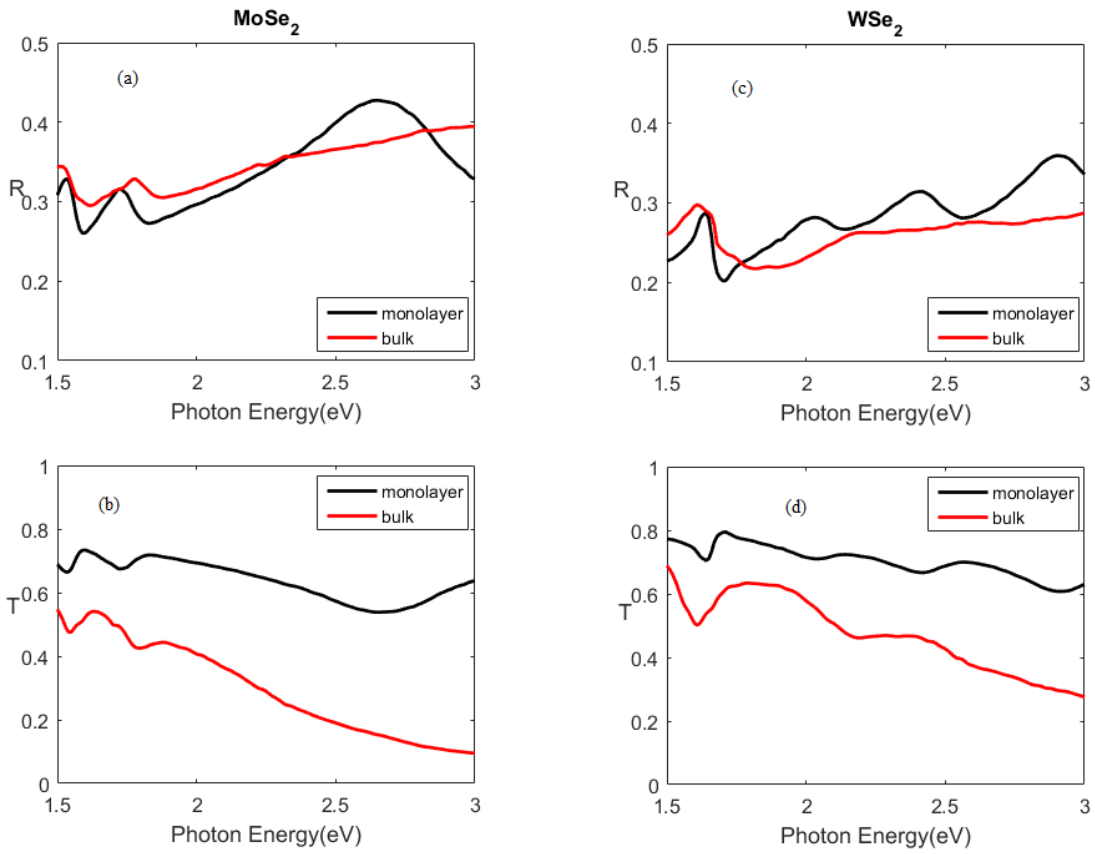

Figure 5.8 Simulated reflectance and transmittance spectra of monolayer and bulk TMDCs on fused silica.

As seen from Figure 5.9, the maximum value of Absorptance (A) for monolayer $MoSe_2$ and WSe_2 on fused silica are 3.57% and 3.43%, respectively. The maximum value of A for bulk $MoSe_2$ and WSe_2 on fused silica are 51.06% and 43.7%, respectively. These values are almost in accordance with the optical properties obtained for suspended monolayer and bulk $MoSe_2$ and WSe_2. However, the presence of a substrate leads to a change in magnitude of R, T and A for a multilayer case.

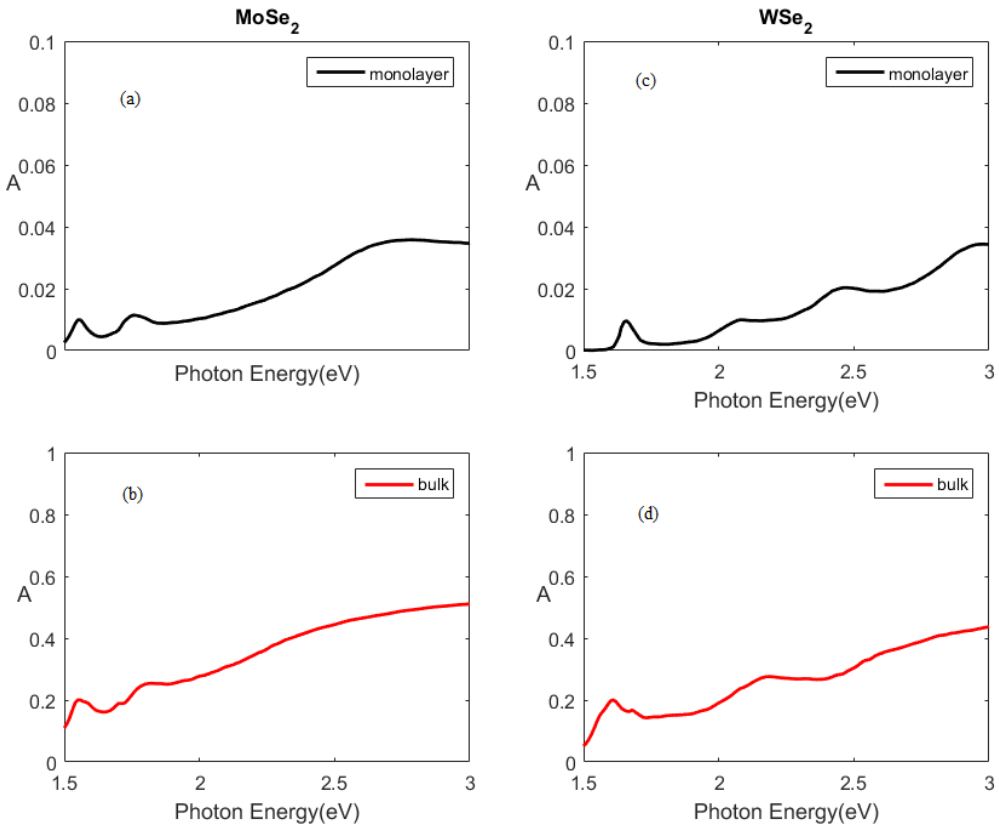

Figure 5.9 Simulated absorptance spectra of monolayer and bulk TMDCs on fused silica.

5.5 Optical Band Gap of Monolayer $MoSe_2$ and WSe_2

The nature of the band gap, direct or indirect, is generally determined by absorption spectroscopy [29]. While a variety of approaches to the determination of energy gap of semiconductors are discussed in the literature [30], the various functional forms of the spectral dependence of the absorption coefficient have been utilized to determine the value of the band gap as well as its nature – direct or indirect. If a plot of α^2 versus $\hbar\nu$ leads to a straight line, it is deemed a direct band gap. The band gap is evaluated by extrapolating the α^2 versus $\hbar\nu$ straight line to $\alpha = 0$ axis. However, a plot of $\alpha^{1/2}$ versus $\hbar\nu$, leading to a straight line, is inferred as an indirect band gap. This indirect band gap is estimated by extrapolating the $\alpha^{1/2}$ versus $\hbar\nu$ straight line to $\alpha=0$ axis.

In earlier sections, the electronic band gap of $MoSe_2$ and WSe_2 was discussed. The optical band gap values determined in this study are smaller than the reported electronic band gap values. This is due to the additional energy absorbed by an electron while making a transition from the valence band to the conduction band. This leads to a difference in the coulomb energies of the two systems (excitation spectroscopy and tunneling spectroscopy) which therefore causes changes in the optical band gaps and electronic band gaps.

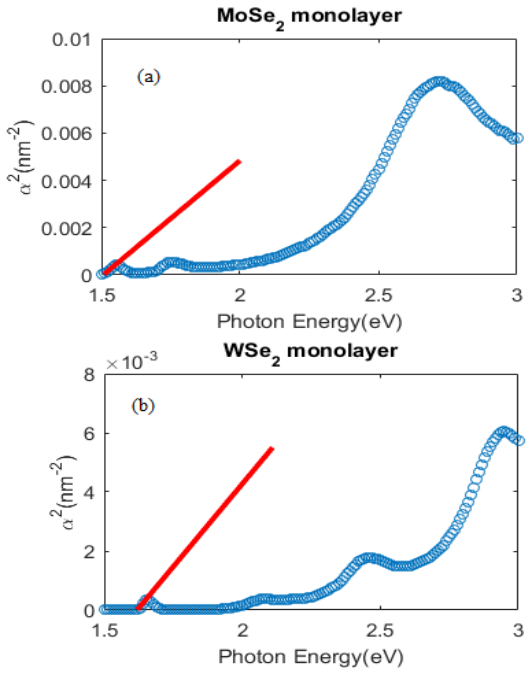

Figure 5.10 Optical band gap of monolayer $MoSe_2$ and WSe_2.

As seen from Figure 5.10, a straight line is observed which corresponds to the first peaks of both monolayer TMDCs; this shows that the monolayer TMDCs have direct band gaps. The values of the optical band gap of monolayer TMDCs were obtained by solving the equations to the straight lines. The optical band gaps of monolayer $MoSe_2$ and WSe_2 were 1.51 eV and 1.62 eV, respectively.

CHAPTER 6

APPLICATIONS OF $MoSe_2$ AND WSe_2

The electronic, electrical and optical properties help us understand the potential applications of $MoSe_2$ and WSe_2 in various industries. The presence of a direct and indirect band gaps make them ideal candidates for optoelectronic devices, field-effect transistors, heterostructure devices etc. A few existing applications of these materials has been discussed in this chapter.

6.1 Field-Effect Transistors

The field-effect transistor (FET) is a transistor that uses an electric field to control the shape and hence the electrical conductivity of a channel of one type of charge carrier in a semiconductor material. FETs are also known as unipolar transistors and as they involve single-carrier-type operation. Conductivity of a non-FET transistor is regulated by the input current (the emitter to base current) and so has a low input impedance, a FET's conductivity is regulated by a voltage applied to a terminal (the gate) which is insulated from the device. The applied gate voltage imposes an electric field into the device, which in turn attracts or repels charge carriers to or from the region between a source terminal and a drain terminal. The density of charge carriers in turn influences the conductivity between the source and drain. Figure 6.1 shows the cross section of a typical Metal Oxide Field Effect Transistor (MOSFET).

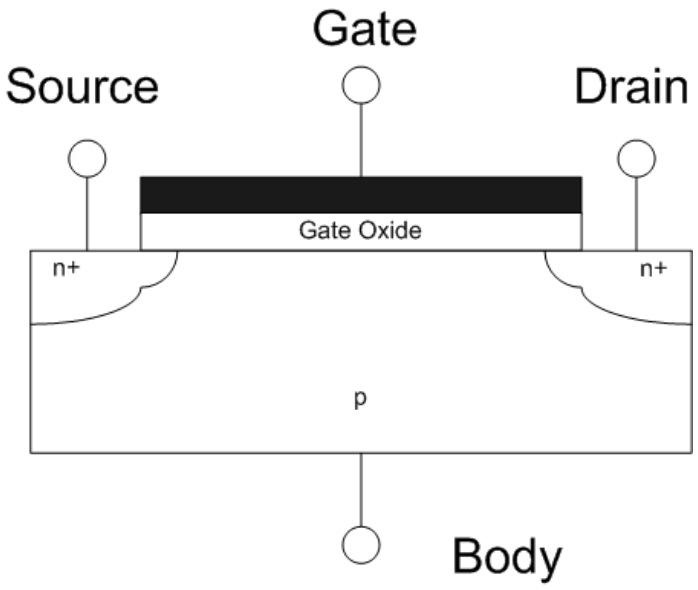

Figure 6.1 Cross section of a typical MOSFET.

These devices are often used in logic circuits due to their ON/OFF operations. Hang et al. [31] report one such application, where transistors based on few layer $MoSe_2$ nanoflakes were fabricated to study their photoelectrical properties. Investigation of these photoelectrical properties enable us to understand their applications as photodetectors, which depend on properties such as high response time, On/Off ratio and gate modulation [31].

$MoSe_2$ nanoflakes of thickness ~2 nm were mechanically exfoliated on a Si/SiO_2 substrate. Earlier reported studies of monolayer and multilayer (bulk) $MoSe_2$ did not give the desired results required to produce an optimum output for photoelectrical applications, hence, few layers of $MoSe_2$ were used in this study. In this study, ~0.65 nm was considered the monolayer thickness; therefore, 2 nm corresponds to trilayers of $MoSe_2$.

Figure 6.2 shows the schematic of side elevation of fabricated back-gated few-layer $MoSe_2$ FET, highly p-doped silicon serves as back gate.

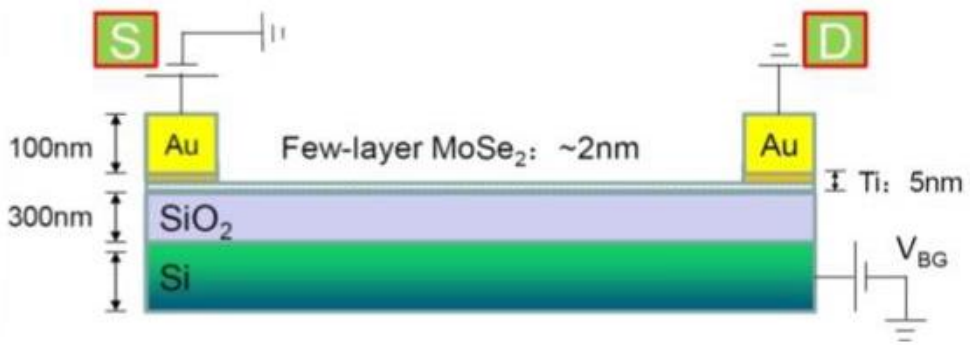

Figure 6.2 Side elevation of fabricated back-gated few-layer $MoSe_2$ FET, highly p-doped silicon serves as back gate.

Source: Hang, Y., Li, Q., Luo, W., He, Y., Zhang, X., & Peng, G. (2016). Photo-Electrical Properties of Trilayer $MoSe_2$ Nanoflakes. Nano, 1650082.

The wavelength of incident light used in this study are 405, 450, 520, 638 and 785 nm, which fall in the visible region of spectra. The incident light intensity is 15 mW for each color [31].

According to the study, the device demonstrated a high On/Off ratio (~10^5) and reasonably high carrier mobility (1.79 cm^2 $V^{-1}s^{-1}$). The PL spectra (PL peak at 1.51 eV) obtained, indicated a strong light-matter interaction in red and near-infrared light [31]. Photo responsivity of the fabricated device was tested and calculated at different laser wavelengths, Hereby, discovering that the device is most sensitive to red light, consistent with the conclusion from PL spectrum. For 638 nm incident laser, the device shows high photo responsivity, quick response time, high EQE, high detection rate and commendable linear working area [31].

Monolayer and few layer WSe_2 also make good field effect transistors, the mobility and On/Off ratio reported by Liu et at. [32] was exceptionally high compared to $MoSe_2$ results obtained by Hang et al [31]. Figure 6.3 shows the schematic of a FET based on WSe_2 grown on BN.

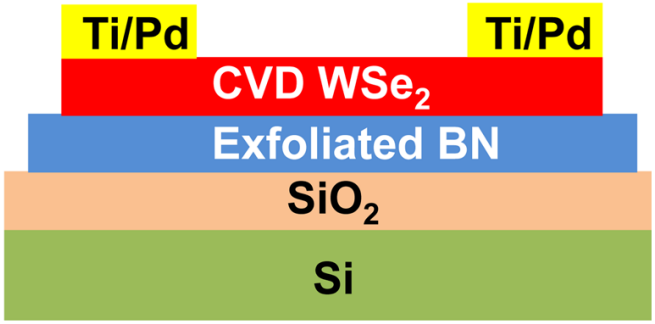

Figure 6.3 Schematic of a FET based on WSe_2 grown on BN.

Source: Liu, B., Ma, Y., Zhang, A., Chen, L., Abbas, A. N., Liu, Y., & Zhou, C. (2016). High-Performance WSe_2 Field-Effect Transistors via Controlled Formation of In-Plane Heterojunctions. ACS nano.

Boron Nitride (BN) was used as a substrate due to its good dielectric properties and its capability of providing dielectric interfaces with very little charge impurities in 2D materials [32].

6.2 Optoelectronics

Since it has been established that 2D TMDCs are optically active materials, a plethora of research is currently being carried out on their applications as optoelectronic devices. LEDs have emerged as solution to most of our energy saving problems in the 21st century. Due to the ultrathin nature and semiconducting properties of TMDCs, these materials could be prospective candidates for LEDs.

Berraquero et al. [33] reported a study involving fabrication of a LED by using monolayer and few layer WSe_2 layered material. The fabricated LED structure was very similar to that reported by Liu et al. [32]. The active region of this device consisted of adjacent monolayer and bilayer active areas, both in contact with the ground electrode. Most of the injected current flow was through the bilayer region. Quantum LED (QLED) operation was observed in the form of highly localized light emission from both the monolayer and the bilayer WSe_2. These localized states were said to lie within the band gap of WSe_2 [33]. The observed emission wavelength range of WSe_2 was said to match rubidium transitions (~780) which could help open up quantum storage possibilities.

6.3 Heterostructures

Heterojunction is the interface that occurs between two layers or regions of dissimilar crystalline semiconductors. These semiconducting materials have unequal band gaps as opposed to a homojunction. It is often advantageous to engineer the electronic energy bands in many solid-state device applications, including semiconductor lasers, solar cells and transistors ("heterotransistors") to name a few. The combination of multiple heterojunctions together in a device is called a heterostructure [34].

According to Furchi et al [35], in the late 70s, TMDCs were used as electrodes of photoelectrovoltaic cells. Their bandgaps, which match well with the solar spectrum, as well as the covalent layer-type nature of these compounds made them promising candidates for efficient solar energy conversion. Solar to electrical power conversion efficiencies up to 10.2% were achieved using WSe_2 and $MoSe_2$ crystals [36]. In this work, multiple van

der Waals heterostructure based solar cells were designed and fabricated. Figure 6.4 shows the schematic of the dual band gap heterostructure.

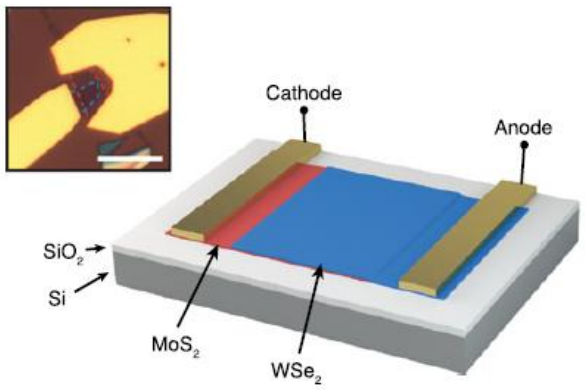

Figure 6.4 Three-dimensional schematic view of the dual band gap cells.

Source: Furchi, M. M., Zechmeister, A. A., Hoeller, F., Wachter, S., Pospischil, A., & Mueller, T. (2017). Photovoltaics in Van der Waals Heterostructures. IEEE Journal of Selected Topics in Quantum Electronics, 23(1), 1-11.

The power conversion efficiency for the cell was found to be of the same order of magnitude (0.1 to 0.2%) which was in agreement with predicted values [37]. The authors of this study expand the idea of bilayer TMDC heterostructures to a three-layer structure. This structure has higher efficiency compared to that of the double layer structure. The high absorption ability of $MoSe_2$ and WSe_2 make them good candidates for solar cell applications, as cited by Furchi et al., [35]. A monolayer of $MoSe_2$ (with a thickness of 0.65 nm) absorbs the same fraction of light as 15 nm of gallium arsenide (GaAs) or 50 nm of silicon (Si) [35]. From this perspective, van der Waals heterostructures seem promising candidates. The amount of raw material needed for the active region is minimal; also, the power conversion densities are expected to be orders of magnitude higher than in conventional cells [35].

CHAPTER 7

CONCLUSIONS

In the study presented above, the electronic, electrical and optical properties of $MoSe_2$ and WSe_2 have been presented. The physical properties of monolayer and bulk $MoSe_2$ and WSe_2 have been studied and distinguished with each other based on literature survey.

Electronic band gaps of monolayer and bulk $MoSe_2$ and WSe_2 were discussed. The optical band gap of monolayer $MoSe_2$ and WSe_2 was simulated using MATLAB. The simulated optical band gap had a smaller value than that of the electronic band gap reported in the literature. This is due to the additional energy absorbed by an electron while making a transition from the valence band to the conduction band. Case studies of various electrical properties such as resistivity, effect of doping and Hall effect were presented and discussed.

The optical constants and optical properties of suspended monolayer and bulk $MoSe_2$ and WSe_2 were simulated by mathematical modelling utilizing MATLAB. The results are in accord with the experimental data and show an appreciable convergence. Temperature dependence studies of the energy gap of monolayer $MoSe_2$ and WSe_2, in the range of 50 to 450 K, have been discussed. Optical properties of these materials on gold, silicon and fused silica substrates are simulated using MATLAB.

REFERENCES

1. Li, X., & Zhu, H. (2015). Two-dimensional MoS_2: Properties, preparation, and applications. *Journal of Materiomics, 1*(1), 33-44.

2. Wilson, J., & Yoffe, A. (1969). The transition metal dichalcogenides discussion and interpretation of the observed optical, electrical and structural properties. *Advances in Physics, 18*(73), 193-335.

3. Wang, Q. H., Kalantar-Zadeh, K., Kis, A., Coleman, J. N., & Strano, M. S. (2012). Electronics and optoelectronics of two-dimensional transition metal dichalcogenides. *Nature nanotechnology, 7*(11), 699-712.

4. Arora, A., Koperski, M., Nogajewski, K., Marcus, J., Faugeras, C., & Potemski, M. (2015). Excitonic resonances in thin films of WSe_2: from monolayer to bulk material. *Nanoscale, 7*(23), 10421-10429

5. Ross, J. S., Wu, S., Yu, H., Ghimire, N. J., Jones, A. M., Aivazian, G., . . . Yao, W. (2013). Electrical control of neutral and charged excitons in a monolayer semiconductor. *Nature communications, 4*, 1474.

6. Wang, Z., Su, Q., Yin, G., Shi, J., Deng, H., Guan, J., . . . Fu, Y. Q. (2014). Structure and electronic properties of transition metal dichalcogenide MX_2 (M= Mo, W, Nb; X= S, Se) monolayers with grain boundaries. *Materials Chemistry and Physics, 147*(3), 1068-1073.

7. Brixner, L. (1962). Preparation and properties of the single crystalline AB_2-type selenides and tellurides of niobium, tantalum, molybdenum and tungsten. *Journal of Inorganic and Nuclear Chemistry, 24*(3), 257-263.

8. Walker, P., & Tarn, W. H. (1990). *CRC handbook of metal etchants*: CRC press.

9. Anedda, A., Fortin, E., & Raga, F. (1979). Optical spectra in WSe_2. *Canadian Journal of Physics, 57*(3), 368-374.

10. El-Mahalawy, S., & Evans, B. (1977). Temperature dependence of the electrical conductivity and hall coefficient in 2H-MoS_2, $MoSe_2$, WSe_2, and $MoTe_2$. *physica status solidi (b), 79*(2), 713-722.

11. Hoffmann, R. (1988). Solids and surfaces: a chemist's view of bonding in extended structures. New York, NY: VCH Publ: Inc.

12. Izyumov, Y. A., & Syromyatnikov, V. N. (2012). *Phase transitions and crystal symmetry* (Vol. 38): Springer Science & Business Media.

13. Peter, Y., & Cardona, M. (2010). *Fundamentals of semiconductors: physics and materials properties*: Springer Science & Business Media.

14. Kumar, A., & Ahluwalia, P. (2012). Electronic structure of transition metal dichalcogenides monolayers 1H-MX_2 (M= Mo, W; X= S, Se, Te) from ab-initio theory: new direct band gap semiconductors. *The European Physical Journal B, 85*(6), 1-7.

15. Mak, K. F., Lee, C., Hone, J., Shan, J., & Heinz, T. F. (2010). Atomically thin MoS_2: a new direct-gap semiconductor. *Physical Review Letters, 105*(13), 136805.

16. Zhu, Z., Cheng, Y., & Schwingenschlögl, U. (2011). Giant spin-orbit-induced spin splitting in two-dimensional transition-metal dichalcogenide semiconductors. *Physical Review B, 84*(15), 153402.

17. Zhang, Y., Ugeda, M. M., Jin, C., Shi, S.-F., Bradley, A. J., Martin-Recio, A., . . . Kim, Y. (2016). Electronic Structure, Surface Doping, and Optical Response in Epitaxial WSe_2 Thin Films. *Nano letters, 16*(4), 2485-2491.

18. Van Zeghbroeck, B. (2011). Principles of electronic devices. University of Colorado.

19. Tongay, S., Zhou, J., Ataca, C., Lo, K., Matthews, T. S., Li, J., . . . Wu, J. (2012). Thermally driven crossover from indirect toward direct bandgap in 2D semiconductors: $MoSe_2$ versus MoS_2. *Nano letters, 12*(11), 5576-5580.

20. Yuan, H., Liu, Z., Xu, G., Zhou, B., Wu, S., Dumcenco, D., . . . Dudin, P. (2016). Evolution of the Valley Position in Bulk Transition-Metal Chalcogenides and Their Monolayer Limit. *Nano letters, 16*(8), 4738-4745.

21. Brumme, T., Calandra, M., & Mauri, F. (2015). First-principles theory of field-effect doping in transition-metal dichalcogenides: Structural properties, electronic structure, Hall coefficient, and electrical conductivity. *Physical Review B, 91*(15), 155436.

22. Thakar, Bhavesh Amrutbhai. Investigations of TMDCs and use in solar cell. Thesis. Hemchandracharya North Gujarat University, Patan, 2011. Shodhganga. Web.2015.<http://shodhganga.inflibnet.ac.in/handle/10603/43941>

23. Li, Y., Chernikov, A., Zhang, X., Rigosi, A., Hill, H. M., van der Zande, A. M., . . . Heinz, T. F. (2014). Measurement of the optical dielectric function of monolayer transition-metal dichalcogenides: MoS_2, $MoSe_2$, WS_2, and WSe_2. *Physical Review B, 90*(20), 205422

24. Mukherjee, B., Tseng, F., Gunlycke, D., Amara, K. K., Eda, G., & Simsek, E. (2015). Complex electrical permittivity of the monolayer molybdenum disulfide (MoS_2) in near UV and visible. *Optical Materials Express, 5*(2), 447-455.

25. Zhang, H., Ma, Y., Wan, Y., Rong, X., Xie, Z., Wang, W., & Dai, L. (2015). Measuring the refractive index of highly crystalline monolayer MoS_2 with high confidence. *Scientific reports, 5*.

26. Liu, H.-L., Shen, C.-C., Su, S.-H., Hsu, C.-L., Li, M.-Y., & Li, L.-J. (2014). Optical properties of monolayer transition metal dichalcogenides probed by spectroscopic ellipsometry. *Applied Physics Letters, 105*(20), 201905.

27. Mattheiss, L. (1973). Band structures of transition-metal-dichalcogenide layer compounds. *Physical Review B, 8*(8), 3719.

28. http://refractiveindex.info/ accessed on June 8 2016.

29. Ravindra, N., Narayan, J., Ance, C., Dechelle, F., & Ferraton, J. (1986). Low-temperature optical properties of hydrogenated amorphous silicon. *Materials Letters, 4*(8), 343-349.

30. Ravindra, N., & Narayan, J. (1987). Optical properties of silicon related insulators. *Journal of applied physics, 61*(5), 2017-2021.

31. Hang, Y., Li, Q., Luo, W., He, Y., Zhang, X., & Peng, G. (2016). Photo-Electrical Properties of Trilayer $MoSe_2$ Nanoflakes. *Nano*, 1650082.

32. Liu, B., Ma, Y., Zhang, A., Chen, L., Abbas, A. N., Liu, Y., . . . Zhou, C. (2016). High-Performance WSe_2 Field-Effect Transistors via Controlled Formation of In-Plane Heterojunctions. *ACS nano*.

33. Berraquero, C. P., Barbone, M., Kara, D. M., Chen, X., Goykhman, I., Yoon, D., . Taniguchi, T. (2016). Atomically thin quantum light emitting diodes. *arXiv preprint arXiv:1603.0879.*

34. Colinge, J.-P., & Colinge, C. A. (2005). *Physics of semiconductor devices*: Springer Science & Business Media.

35. Furchi, M. M., Zechmeister, A. A., Hoeller, F., Wachter, S., Pospischil, A., & Mueller, T. (2017). Photovoltaics in Van der Waals Heterostructures. *IEEE Journal of Selected Topics in Quantum Electronics, 23*(1), 1-11.

36. Kline, G., Kam, K., Canfield, D., & Parkinson, B. (1981). Efficient and stable photoelectrochemical cells constructed with WSe_2 and $MoSe_2$ photoanodes. *Solar Energy Materials, 4*(3), 301-308.

37. Bernardi, M., Palummo, M., & Grossman, J. C. (2013). Extraordinary sunlight absorption and one nanometer thick photovoltaics using two-dimensional monolayer materials. *Nano letters*, *13*(8), 3664-3670.

APPENDIX

MATLAB Code 1.

Code used for determining optical constants ‘n’ and ‘k’ for monolayer and bulk $MoSe_2$ and WSe_2:

```
photonenergyev1= photonenergyev1(~isnan(photonenergyev1));
photonenergyev2= photonenergyev2(~isnan(photonenergyev2));
epsilon1= epsilon1(~isnan(epsilon1));
epsilon2= epsilon2(~isnan(epsilon2));
photonenergyevfit=1.50:0.01:3;
epsilon1fit=interp1(photonenergyev1,epsilon1,photonenergyevfit,'spline');
epsilon2fit=interp1(photonenergyev2,epsilon2,photonenergyevfit,'spline');
n=[];
for i=1:1:151
   p = [4 0 -4*epsilon1fit(i) 0 -epsilon2fit(i)^2];
   x=roots(p);
   for ii=1:length(x)
      if x(ii)>0 & isreal(x(ii));
         n(i)=x(ii);
         k(i)=epsilon2fit(i)/(2*n(i));
      end
   end
```

```
end
output=[photonenergyevfit',n',k',epsilon1fit',epsilon2fit'];
```

MATLAB Code 2.

Code used for determining optical properties (R, T and A) of monolayer $MoSe_2$ and WSe_2:

```
%%This program is to calculate R and T for 2-layer structure with two kinds
%%of material.
%%Inputs are:
%%n1 the real part of refraction index for the material in first layer that is MoSe2 or
WSe2;
%%k1 the imaginarydpart of refraction index for the material in first layer;
%%t1 the thickness of the material in first layer(in nm);
%%n2 the realpart of refraction index for the material in second layer that is SILICON;
%%k2 the imaginarydpart of refraction index for the material in second layer
%%t2 the thickness of the material in second layer (in nm);
%%photonenergyevfit the fitted photonenergy range, this should be same for
%%both of the material.
%%The size of n1 n2 k1 k2 and photonenergyevfit should be the same, and
%%they should be in a row matrix.
N=size(photonenergyevfit,1);
Rmat=[];
R=[];
RSi=[];
```

```
T1=[];
T2=[];
alpha1=[];
alpha2=[];
T=[];
A=[];
Amat=[];
Wavelength = photonenergyevfit.\1240
for i=1:151;
   Rmat(i)= ((n1(i)-1)^2+k1(i)^2)/...
      ((n1(i)+1)^2+k1(i)^2)
    RSi(i)= ((n2(i)-1)^2+k2(i)^2)/...
      ((n2(i)+1)^2+k2(i)^2)
   R(i)=((n1(i)-n2(i))^2+k1(i)^2)/...
      ((n1(i)+n2(i))^2+k1(i)^2);
   alpha1(i)= (4*pi*k1(i))/wavelength(i);
   alpha2(i)= (4*pi*k2(i))/wavelength(i);
   T1(i)= (1-Rmat(i))*exp(-alpha1(i)*0.70);
   T2(i)= (1-R(i))*exp(-alpha2(i)*650000);
   T(i)=T1(i)*T2(i);
   Amat(i)= (1-Rmat(i)-T1(i))*100;
   A(i)= (1-R(i)-T(i))*100;
end
```

```
Output=[photonenergyevfit;R;T1;T2;T;A;Rmat;Amat;RSi;alpha1;alpha2]';
```